University of Alberta

Characterization of copper supported on titanosilicates for room temperature H_2S adsorption

by

Aida Tavana

A thesis submitted to the Faculty of Graduate Studies and Research
in partial fulfillment of the requirements for the degree of

Master of Science
in
Chemical Engineering

Department of Chemical and Materials Engineering

Spring 2012
Edmonton, Alberta

Dedicated to my parents

Abstract

Hydrogen sulfide (H_2S) is a major contaminant of industrial gas streams. Amongst the various methods used for its removal, adsorption by metal oxides is the most promising. Copper oxide (CuO) is shown to have superior H_2S removal capability at room temperature. H_2S removal at room temperature is useful when the gas stream's temperature is low and in applications such as on-board fuel processing of proton exchange membrane fuel cells.

The addition of supports improves the adsorption capacity and utilization of copper species. In this study, Engelhard titanosilicates (ETS-2, ETS-4 and ETS-10) were chosen as supports due to their high surface area and ion-exchange capacities. Copper species were dispersed on the supports via ion-exchange.

The H_2S adsorption potential of Cu-ETS-2, Cu-ETS-4 and Cu-ETS-10 versus commercial H_2S scrubbers was investigated. Cu-ETS-2 was found to be the most effective adsorbent at room temperature due to its high external surface area and high dispersion of copper species.

Acknowledgments

I would like to acknowledge my supervisor Prof. Steven Kuznicki for his guidance, support and great encouragement during my studies. I would also like to thank my examining committee, Dr. Zaher Hashisho, Dr. Greg Dechaine and Dr. Larry Unsworth for their invaluable comments and suggestions. I give special thanks to Dr. James Sawada for his guidance and valuable advice.

I sincerely thank Lan Wu, An Weizhu, Tong Qiu, and every member of our research group, for their general contributions and perspectives. I also thank Diane Caird, De-ann Rollings, Dimitre Karpuzov, Roham Eslahpazir for their assistance with various analytical instruments and Mrs. Albana Zeko for her assistance with manuscript development.

Financial support from Helmholtz Alberta Initiative (S.M.K.) is gratefully acknowledged.

Table of Contents

List of Tables

List of Figures

Nomenclature

Abbreviations

AAS	Atomic absorption spectrophotometry
AC	Activated carbon
BE	Binding energy
BET	Brunauer, Emmett, Teller
DSC	Differential scanning calorimetry
EDS/EDX	Electron dispersive X-ray spectroscopy
ETS-2	Engelhard titanosilicate-2
ETS-4	Engelhard titanosilicate-4
ETS-10	Engelhard titanosilicate-10
eV	Electronvolt
FPD	Flame photometric detector
GC	Gas chromatograph
KE	Kinetic energy
PEMFC	Proton exchange membrane fuel cells
ppm	Parts per million
SAED	Selected area electron diffraction
SEM	Scanning electron microscopy

TA	Thermal analysis
TEM	Transmission electron microscopy
TGA	Thermogravimetric analysis
XRD	X-ray diffraction
XPS	X-Ray photoelectron spectroscopy

Symbols

°	Degree
A	Surface area
Å	Angstrom
θ	Diffraction angle
λ	Wavelength
υ	Frequency
ΔG	Free energy change
ΔE	Energy change
a_m	Molecular area of the adsorbate
C	BET constant
d	Distance between two crystal planes
h	Plank’s constant
P_0	Saturation pressure
P	Total pressure
V_m	Monolayer volume
V	Volume

Chapter 1. Introduction

1.1. Sources of Hydrogen Sulfide

Hydrogen sulfide (H_2S) is present in nature in hot springs and volcanic gases. It is also naturally produced as a result of bacterial digestion of organic matter and human and animal wastes in environments without oxygen. Natural gas is another major source of substantial amounts of H_2S.

Human activities have become a significant source of hydrogen sulfide emission. Coal which, depending on its source, has 0.1 to 6 wt.% sulfur content releases H_2S during coal gasification processes.[1] As a result Syngas, which is the main product of gasification for electric power generation, is mixed with H_2S. This product should be cleaned of H_2S in order to prevent poisoning of separation membranes and corrosion of gas turbines and pipelines that are used later in the process.

Crude oil is also a source of sulfur which, depending on the source, can contain 0.2 to 4 wt.% sulfur.[1] The sulfur in crude oil is present in different forms such as, organic sulfur compounds, H_2S and small amounts of elemental sulfur.

1.2. The Necessity of H_2S Removal

In nature, H_2S can be the source of acid rain which occurs when H_2S is oxidized in air (sulfur dioxide) and reacts with water. Acid rain can cause acidification of lakes and soils with harmful consequences for the fishes and trees. It can also increase the rate of corrosion of metallic structures (e.g. bridges).

In industry a nickel or alumina catalyst, used in steam reforming processes, can be poisoned by the H_2S contents of natural gas. In addition, sulfur levels higher than 3 ppm can cause corrosion in the pipelines used for transporting natural gas, therefore reducing the plant's lifetime.[2]

Fuel cells, which are promising candidates for electrical power generation, use hydrogen as their fuel. The pure hydrogen gas is mostly provided by natural gas, but can also be derived from coal, biomass, alcohols and petroleum derivatives, gasoline and diesel. Natural gas H_2S content is reduced to meet environmental regulations, but the remaining H_2S content is still problematic for fuel cell applications. Since anode catalyst of fuel cells can be poisoned by even 0.1-1 ppm H_2S, the produced syngas should be scavenged completely before being applied as a fuel for fuel cells.[3]

The membranes which are used for separation of syngas are also susceptible to H_2S concentrations, and should be protected by H_2S scavengers.

Last but not least H_2S is an odorous, toxic gas that can be hazardous to human health. At low concentrations, it can be detected by humans by a distinctive rotten egg odor. Higher concentrations however, and long exposure may deaden the sense of smell.

The following table summarizes the effects of different exposure levels of H_2S on human health.[4]

Table 1-1 Effects of H_2S exposure at different levels[4]

Concentration (ppm)	Effects of Exposure
0.13	This is the odour threshold. Odour is unpleasant. Sore eyes.
4.6	Strong intense odour, but tolerable. Prolonged exposure may deaden the sense of smell.
10-20	Causes painful eye, nose and throat irritation, headaches, fatigue, irritability, insomnia, gastrointestinal disturbance, loss of appetite, dizziness. Prolonged exposure may cause bronchitis and pneumonia.
30-100	Sickeningly sweet smell noted.
50	May cause muscle fatigue, inflammation and dryness of nose, throat and tubes leading to the lungs. Exposure for one hour or more at levels above 50 ppm can cause severe eye tissue damage. Long-term exposure can cause lung disease.
100-150	Loss of smell, stinging of eyes and throat. Fatal after 8 to 48 hours of continuous exposure.
200-250	Nervous system depression (headache, dizziness and nausea are symptoms). Prolonged exposure may cause fluid accumulation in the lungs. Fatal in 4 to 8 hours of continuous exposure.
250-600	Pulmonary edema (lungs fill with fluid, foaming in mouth, chemical damage to lungs).
300	May cause muscle cramps, low blood pressure and unconsciousness after 20 minutes.
300-500	May be fatal in 1 to 4 hours of continuous exposure.

500	Paralyzes the respiratory system and overcomes victim almost instantaneously. Death after exposure of 30 to 60 minutes.
700	Paralysis of the nervous system
1000	Immediately fatal.

It is apparent that H_2S, even at low levels, can cause health hazards for people exposed to it, such as workers in sewage treatment plants, manholes, tunnels and chemical laboratories.

1.3. Current Techniques for H_2S Removal

1.3.1. Absorption in Liquids

Liquids that are used for H_2S absorption include alkanolamines, aqueous ammonia and alkaline salt solutions.

1.3.1.1. Alkaloamines

Monoethanolamine, $HOCH_2CH_2NH_2$ (MEA) is the most widely used alkaloamine for removing H_2S. The gas stream containing H_2S is passed through a packed column, while the clean MEA solution is passed counter currently to the gas flow. The MEA rich in H_2S is then regenerated in a stripping column by transferring the sulfur back to the gas phase. The sulfur, which is in H_2S form, is then cooled down to remove water vapor and restrained for further processing. This process is also applicable for removing CO_2 out of gas streams.[1]

1.3.1.2. Ammonia Solution

In this process H_2S is absorbed in an aqueous ammonia solution as per following reactions:

$$NH_{3(aq)} + H_2S \leftrightarrow [NH_4]^+_{(aq)} + [HS]^-_{(aq)} \qquad \text{Reaction 1.1}$$

$$2NH_{3(aq)} + H_2S \leftrightarrow 2[NH_4]^+_{(aq)} + S^{2-}_{(aq)} \qquad \text{Reaction 1.2}$$

The absorption column is similar to the one used in an alkaloamines process.[1]

1.3.1.3. Alkaline Salt Solutions

Sodium and potassium carbonate or phosphate solutions have been widely used for H_2S removal.

The Seaboard process, which was the first regenerative liquid based process for H_2S removal in industrial scale, could absorb H_2S in sodium carbonate solution.[1] The regenerated H_2S was then oxidized to SO_2 by combustion and released to atmosphere, causing environmental concerns.

Absorption into liquid methods can experience operating difficulties such as high solvent losses, failure to meet sweet gas specification, foaming, corrosion , fouling of equipment and contamination of the solution. Nevertheless, the reduction of hydrogen sulfide’s concentration from percentage to ppm levels is readily achieved by these methods. The challenging problem is to remove the last traces of H_2S from the process stream that has been the focus of this work.

1.3.2. The Claus Process

The Claus Process, which was invented over 100 years ago, is the most significant gas desulfurizing process for recovering elemental sulfur from gaseous hydrogen sulfide.

The Claus Process consists of two steps: thermal and catalytic. In the thermal step, H_2S reacts in a substoichiometric combustion reaction at temperatures above 850 °C while the elemental sulfur precipitates in the downstream process gas cooler.

$$H_2S + 1.5\, O_2 \leftrightarrow H_2\, O + SO_2 \qquad \text{Reaction 1.3}$$

$$2H_2S + SO_2 \leftrightarrow 3S \downarrow + 2H_2 \qquad \text{Reaction 1.4}$$

In the catalytic step, the Claus reaction (Reaction 1.4) continues with activated Al_2O_3 or TiO_2. The remaining H_2S reacts with SO_2 (formed during combustion in the reaction furnace) and further boost the sulfur yield.

The Claus Process, in addition to the high efficiency (94% - 97%) has a relatively small ecological impact, when coupled with a tail-gas treatment unit. However, the H_2S levels in the Claus process cannot be reduced to ppm levels due to the equilibrium limitation of Reaction 1.4.[1]

1.3.3. Activated Carbon

Activated carbon (AC) is used as an absorbent for H_2S removal, due to its high specific surface area and porous structure. Although, it can adsorb H_2S by physisorption or chemisorption, it is not considered a good candidate for H_2S

removal due to its low capacity.[3] However, the adsorptive capacity of AC can be improved by impregnation with copper or potassium hydroxide. Huang et al. has shown that AC impregnated with copper has 10 times more H_2S capacity than virgin AC.[5]

1.3.4. Metal Oxides

Hydrogen sulfide can be removed through the reaction with metal oxides in a wide range of temperatures.

1.3.4.1. High Temperature

In 1976, Westmoreland et al. conducted a thermodynamic survey of 28 elements of the periodic table and found that Fe, Zn, Mo, Mn, V, Ca, Sr, Ba, Co, Cu and W oxides are all potential candidates for high temperature (>350°C) desulfurization.[6] Elsevier et al. showed that for Mo and W oxides metal carbides are formed at moderate temperatures, therefore, these compounds cannot be good candidates for desulfurization.[7]

Among the potential metal oxides, zinc oxide has been extensively studied as the most favourable candidate for desulfurization purposes. Zinc oxide adsorbs H_2S via the following reaction:

$$ZnO + H_2S \rightarrow ZnS + H_2O \qquad \text{Reaction 1.5}$$

The required activation energy is provided by the high reaction temperatures (> 200°C) [3], while at room temperature the reaction rate is reduced considerably. In its applicable temperature range, and in the presence of water, the hydrogen sulfide concentration cannot be reduced below 0.1 ppm due to equilibrium limitations.[8]

In order to enhance the adsorptive performance of metal oxides strategies such as doping with other metals have been used. Ayala et al. tested zinc ferrite's desulfurization potential of coal gases at 538°C, in 50 cycles of adsorption and regeneration.[9] Mixed oxides of copper with Cr, Ce, Al, Mg, Mn, Ti and Fe were also investigated and it was found that CuO-Cr_2O_3 and Cu-CeO_2 were the most efficient desulfurization adsorbents at 650°C.[10]

In order to enhance the utilization of active chemicals (metals/metal oxides) and their H_2S breakthrough capacities, increasing the surface area is required. This can be accomplished by loading the active chemicals on different supports such as Al_2O_3, TiO_2, SiO_2, and zeolites. This strategy increases the surface area as well as improves structural stability.

One study compared pure zinc oxide with zinc titanates and concluded that zinc titanate reduces more slowly to volatile zinc, thus it can be applied at higher temperatures.[11] Tzu-Hsing Ko et al. compared adsorption capacities of Mn, Fe, Cu, Co, Ce and Zn supported on γ-Al_2O_3 for H_2S removal in syngas at 500°C-700°C and reported 100% utilization for copper and manganese.[12] Another study reported that when copper, molybdenum and manganese are supported on SP-115 zeolite an increase in the mechanical strength of the adsorbents is observed.[13] Kyotani et al. studied copper supported on SiO_2 and natural zeolite (with major phases of mordenite and clinoptilolite) and compared it to pure copper oxide.[14]

The study found almost the same breakthrough capacities at 600°C for copper supported on SiO_2 (15 wt.% copper) and zeolite (20 wt.% copper) as of for pure copper oxide. The study also showed that pure copper oxide had the lowest reactivity for sulfidation due to the formation of a dense copper sulfide phase.

1.3.4.2. Room Temperature

H_2S removal at room temperature has received less attention than high temperature removal but it has the advantage of substantially reduced processing costs. In addition the room temperature removal of H_2S is technically attractive, as it is required for on-board fuel processing of proton exchange membrane fuel cells (PEMFC).

Fuel cells are the emerging technology for power generation with potential applications in transportation and stationary and portable power generations. PEMFCs are the most widely researched and developed type of fuel cells; they operate at low temperatures (up to 80°C) and require ultra-high purity hydrogen to function at peak efficiency and lifetime. Development of on-board fuel processing is the most recent challenge for PEM fuel cells applications.[15,16] In on-board fuel processing the liquid hydrocarbon is converted to reformate, supplying hydrogen for fuel cells. However, the remaining sulfur content in liquid fuels is converted to H_2S at this step. Since the anode Pt catalysts in PEMFC can be poisoned by H_2S levels as low as 0.1 ppm an in-line fuel filter is required to polish the reformate and protect PEM fuel cells.

A comparative study of different metal oxides (Ag, Cu, Zn, Co,Ni, Ca, Mn and Sn) has been conducted by Mei Xue et al.[17] The study showed that the hydrous CuO has the highest H_2S uptake capacity using 10 ppm H_2S in N_2 at room temperature. In another study Yang et al. doped ZnO/SiO_2 with eight different transition metals and compared the H_2S capacities with ZnO/SiO_2 at room temperature. The copper doped ZnO/SiO_2 had the highest H_2S capacity, which was double that of ZnO/SiO_2.[8] Baird et al. also showed that copper and cobalt dopants enhance the sulfur removal capacity of ZnO at room temperature.[2]

At low temperatures H_2S can only react with the first monolayer of metal oxides [2], thus applying supports that increase the surface area can significantly enhance the utilization of metal oxides at low temperatures. In the following section different types of molecular sieves are evaluated as potential supports of active chemicals for H_2S adsorption.

1.4. Molecular Sieves Applications for H_2S Adsorption

1.4.1. Classical Molecular Sieves (Zeolites)

Zeolite molecular sieves are widely used in the chemical processing industry for applications ranging from adsorption to catalysis and ion-exchange.[18] These inorganic materials were first discovered by Axel Cronstedt in 1756.[19] Zeolites have three-dimensional frameworks that bring about their unique characteristics. They have crystalline, micro-porous, hydrated aluminum silicate structures of $[SiO4]^{4-}$ and $[AlO4]^{5-}$ tetrahedras linked together, forming open cages connected by pore openings ranging from 2.5 to 10 Å. Each AlO_4 unit in the framework carries a negative charge that is balanced by non-framework cations like sodium [Na^+], potassium [K^+], or [Ca^{2+}]. These cations can be replaced by other cations via ion exchange. A zeolite framework is illustrated in the following figure:

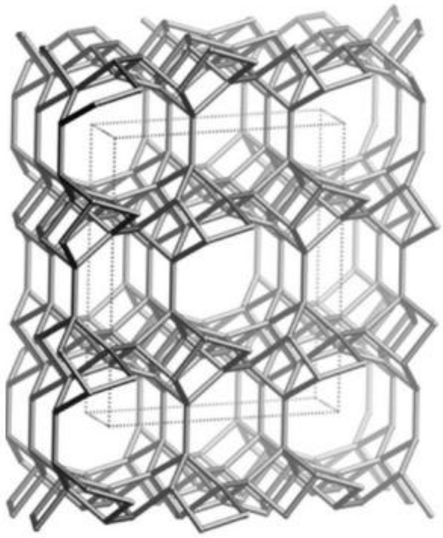

Figure 1-1 Natural zeolite (Clinoptilolite) framework [20]

Due to the high surface area and ion exchange capability of zeolites, active chemicals can be exchanged into their framework and applied for H_2S removal applications. However the presence of water vapour in gas streams would render the zeolite-based adsorbents inactive toward H_2S. This is caused by the capillary condensation that occurs in channels within the framework. Zeolite based adsorbents with small pore size can have reduced activity due to pore blockage as well. It has been reported that in case of SP-115 with a pore size of 5.4 Å, not all the cations are accessible to H_2S gas molecules.[14] This is caused by the sulfur over layers formed during sulfidation which blocks the pores and hinders the complete utilization of deposited cations.

1.4.2. Mixed Coordination Molecular Sieves

1.4.2.1. ETS-4 and ETS-10

Mixed octahedral/ tetrahedral titanium silicate molecular sieves are composed of three-dimensional network of interconnecting channels. Zorite is an example of a natural molecular sieve first discovered in trace amounts on the Siberian Tundra in 1973, and composed of titanosilicate frameworks.[21] Engelhard titanosilicate molecular sieves ETS-4 and ETS-10 are the synthetic forms of Zorite minerals, and were patented in 1989.[22] They can be identified by the following mole ratios of oxides:

$$1.0 \pm 0.25\ \mathrm{M_{2/n}O : TiO_2 : y\ SiO_2 : z\ H_2O}$$

Wherein M is at least one cation having a valence of n, y ranges from 1.0 to 10.0, and z from 0 to 100. In a preferred embodiment, M is a mixture of alkali metal cations, particularly sodium and potassium, and y is at least 2.5 and ranges up to about 5. The framework of ETS-10 is shown in Figure 1-2.

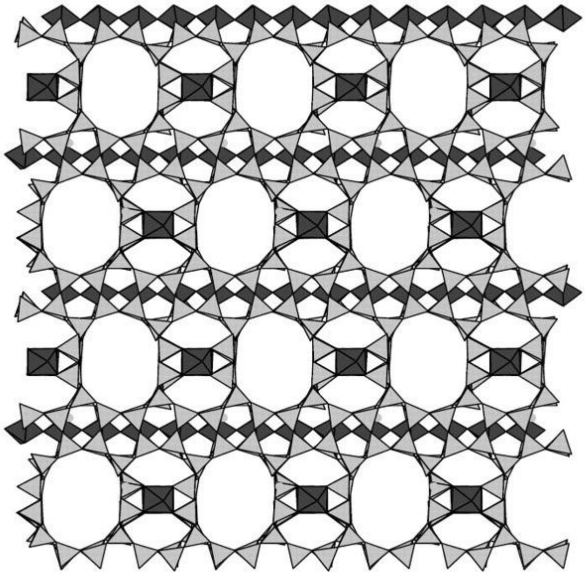

Figure 1-2 ETS-10 framework [23]

ETS- 4 and ETS-10 have been used for different purposes from catalysis to adsorption and ion-exchange.[18] These high surface area ion exchangers provide atomic dispersion of active chemicals in their microporous framework and this allows for higher utilization of the active chemical.

ETS-4 and ETS-10 also have similar disadvantages. The pore blockage may occur in small pored titanosilicates and reduce the active chemical utilization. Also, the presence of pores and channels in ETS-4 and ETS-10 structure creates a problem in humid gas streams as the pore system will fill up with liquid water due to capillary condensation.

1.4.2.2.ETS-2

Engelhard titanosilicate-2 (ETS-2), patented in 1989 [22], differs from ETS-4 and ETS-10 in some key aspects. Unlike ETS-4 and ETS-10 this material lacks the porosity that defines its molecular sieve relatives. ETS-2 is a form of sodium titanate which, through the addition of silica in the synthesis process, becomes a highly effective ion exchanger. The framework of ETS-2 is semi-crystalline and its high surface area is driven by its particle size which, unlike ETS-4 and -10 is in the nanometer range. Since the surface area for ETS-2 is entirely external (it has no pores and channels), it does not suffer from pore blockage or capillary condensation issues.

1.5. Thesis Overview

Based on the superior H_2S adsorption performance of Cu-based compounds at room temperature, a novel Cu-based adsorbent was prepared using a high surface area titanosilicate (ETS-2) as the support. This novel adsorbent was tested for the adsorption of low concentrations of H_2S at room temperature and the capacity and copper utilization was compared to commercial, low temperature H_2S adsorbents as well as copper-exchanged ETS-4 and ETS-10. This work also investigates the effect of activation temperature on the H_2S capacity of Cu-ETS-2.

Chapter two describes the preparation procedure of Cu-ETS-2/4/10 and adsorption test conditions followed by the description of applied characterization techniques. In chapter three, morphology, structure and chemical properties of synthesized adsorbents are discussed by means of different characterization tests (XRD, XPS, EDX, AAS, TEM, SEM and Surface area measurements). This chapter also focuses on the effect of activation temperature on Cu-ETS-2 properties, investigated by TGA/DSC, XRD and surface area measurements. Chapter four discusses the breakthrough capacity and copper utilization of Cu-

ETS-2 versus Cu-ETS-4, Cu-ETS-10 and commercial samples. The thesis concludes with chapter five, which highlights the key discoveries of this work.

Chapter 2. Methods and Materials

2.1. Adsorbent Preparation

ETS-2, ETS-4 and ETS-10 were synthesized hydrothermally as cited in the literature.[22] The method for ETS synthesis involves addition of sources of silica, sources of titanium, and sources of alkalinity such as sodium and/or potassium hydroxide and water. Sources of potassium fluoride can be used as optional to improve the solubility of a solid titanium source. Sodium silicate (28.7% SiO_2, 8.9% Na_2O) was the source of silica in ETS-2, ETS-4 and ETS-10. The source of titanium for ETS-2 was solid TiO_2, while solubilised $TiCl_3$ was used for ETS-4 and ETS-10 synthesis.

The ion exchange procedure was performed by mixing the as-synthesized powdered material with a copper nitrate salt solution. The weight proportion of adsorbent (ETS-2/4/10) to salt and water was 1:2:10. The salt was dissolved prior to adding the adsorbent and agitating the mixture. The sealed vessel containing the slurry was then placed in an oven at 80°C for approximately 18 hours. Afterward, the exchanged samples were filtered and washed with de-ionized water and dried at 80 °C overnight. Adsorbent granules were generated by mixing the Cu-exchanged powder with Ludox HS-40 colloidal silica (10:4 wt/wt ratio). The relatively dry mixture was placed in a cylindrical mold (2.54 cm diameter) and compressed in an axial press to a pressure of 6 metric tons for about 1 minute. The disk formed at this step was crushed and sieved to obtain 20-50 mesh particles. Prior to analysis, samples were heated in a muffle furnace. The samples were activated in air at a heating rate of ~4°/min with an isothermal dwell of 2 hrs.

Commercial samples (BASF Chemical Company) of 36 wt.% CuO (R3-11G), 40 wt. % CuO + 40 wt. % ZnO (R3-12) and pure zinc oxide (ZnO) were sieved to 20-50 mesh particles and used as received.

2.2. H_2S Adsorption Test

A sample of 50 mg of the pelletized adsorbent was packed between plugs of glass wool in a stainless steel column of 4 cm length and 0.38 cm inside diameter. The adsorbent was exposed to a continuous flow of 100 ml/min of the 10 ppm H_2S (balance N_2) mixture. The flow rate was controlled by needle valves and was measured using a bubble flow meter. The outlet of the bed was connected to a Gas Chromatograph (GC) equipped with a FPD detector and the H_2S concentration was monitored continuously during the experiments at 4 minute intervals. The breakthrough point was determined when an H_2S concentration of 0.5 ppm was measured at the outlet of the bed.

2.3. Characterization Techniques

In order to gain a better understanding of the structural and chemical properties of adsorbents, different characterization tests were performed.

2.3.1. Surface Area Measurements

The specific surface area of ETS-2 was determined by N_2 adsorption using an Autosorb-1 volumetric system from Quantachrome Instruments. Nitrogen gas is typically used for surface area analysis because it is inexpensive and readily available.

In the volumetric method N_2 is taken into the reservoir while the pressure is monitored on the manometer. The valve between the sample and the reservoir is then opened and some volume of gas is admitted to the sample. Subtracting the "dead space" in the sample bulb and piping connections the volume adsorbed can be determined. The final stabilized pressure is the equilibrium adsorption pressure. An isotherm is generated by sequentially dosing the sample with gas and measuring the pressure decay.[24]

The surface area of the adsorbent is calculated using the BET method. BET stands for Brunauer, Emmett, and Teller, who published the theory in 1938.[25] Assuming that the surface on which the adsorbate is condensing does not restrict the number of adsorbed gas layers, they obtained the following expression:

$$\frac{P}{V(P_0-P)} = \frac{1}{V_m C} + \frac{C-1}{V_m C} \left(\frac{P}{P_0}\right) \qquad \text{Equation 2.1}$$

where V is the adsorbed volume, P is the pressure in the fluid phase and P_0 is the saturation pressure, derived from N_2 isotherm experimental data. By plotting $\frac{P}{V(P_0-P)}$ versus $(\frac{P}{P_0})$ the values of V_m and C are determined from the slope and intercept of the plot, where V_m is the monolayer volume and C is an affinity constant for the adsorbate-adsorbent interaction. Knowing the molecular area of the adsorbate (a_m), the value of the surface area (A) can be calculated directly from V_m.

2.3.2. X-ray Diffraction (XRD)

The crystalline structures of the adsorbents were examined by XRD measurements. The reflections in a powder XRD provide a fingerprint of the material which provides information about the symmetry of the crystal lattice and the samples phase purity.

Crystalline materials consist of planes of atoms that are spaced a distance d apart. In X-ray diffraction, the sample is exposed to beam of X-rays (0.5 Å <wavelength< 2Å).[26] When there is constructive interference from X rays scattered by the atomic planes in a crystal, a diffraction peak is observed (Figure 2-1). Bragg equation relates the beam wavelength to distance between defined planes in crystal phase:

$$n\lambda = 2d \sin\theta \qquad \text{Equation 2.2}$$

where n is an integral value of 1 or greater.

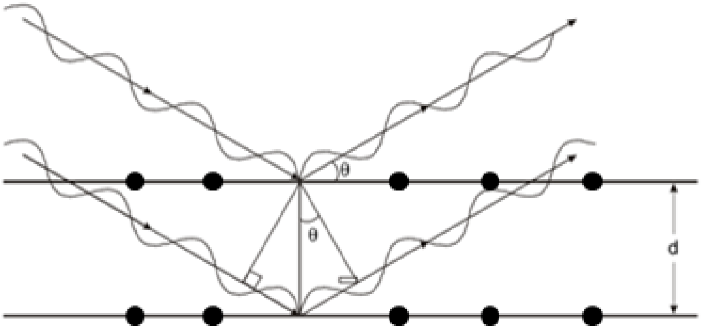

Figure 2-1 X-ray diffraction by atomic planes in the crystal

Experimental X-ray diffraction patterns are collected as a function of 2θ, while the X-ray beam source hits the sample at an angle of θ and the detector collects the exiting beams. The detector measures the intensity of the beam leaving the sample surface.

In this study, the XRD patterns were collected using a Rigaku Geigerflex Model 2173 diffractometer with a cobalt (Co Kα λ =1.79021Å) rotating anode source. The system was equipped with a graphite monochromator to filter the K-beta wavelengths. Samples were ground to a fine powder for XRD tests and the patterns were collected at room temperature.

2.3.3. Transmission Electron Microscopy (TEM)

TEM test was used for probing the morphology and crystallinity of selected components in the samples.

In TEM the source of a highly energetic beam of electrons hits the sample and produces characteristic radiation from the sample.

The most important feature of TEM is its high lateral spatial resolution (better than 0.2 nm "point-to-point” on some instruments) which is caused by using highly focused electron beam as a probe with extremely small wavelength.[26]

The TEM column has an electron gun which is the source for ejecting electron. These emitted electrons are accelerated and focused by means of lenses placed before the specimen (electrostatic and condenser lenses). Another set of lenses are objective lenses which surrounds the specimen and controls the instrumental resolution.

Post-specimen lenses (diffraction, intermediate, projector 1 and projector 2) are placed after the specimen and magnify the signal transferred by the objective lenses, hence magnifying the diffraction pattern or produced image.

The TEM column also has diaphragms and apertures which blocks certain scattered waves and controls the contrast. The most important diaphragm is placed in the back focal plane of the objective lenses, shown in Figure 2-2:

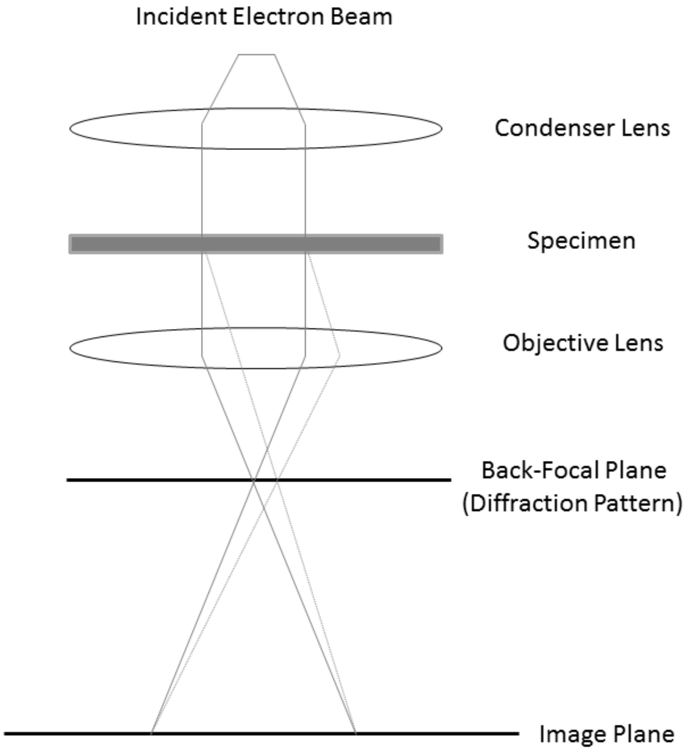

Figure 2-2 Simple schematic of TEM column

TEM offers two modes, diffraction mode and image mode.

In diffraction mode the post-specimen lenses are set to determine the information in transmitted signal at the back focal plane of objective lenses (Figure 2-2). Also, for getting selected area diffraction patterns (SAED) a selected area aperture is used to limit the diffracting volume. The single crystal will produce a spot pattern; a polycrystal will produce a ring pattern, while the amorphous sample will produce haloes in their diffraction patterns.

In image mode, the post-specimen lenses are set to examine the information in the transmitted signal at the image plane of the objective lens (Figure 2-2). The image is produced due to mass contrast, thickness contrast and diffraction contrast.

In TEM the sample must be transparent to the electron beams, thus a thin layer of that is used for analysis (less than 200 nm). In our case, samples in powder form were suspended in methanol and dispersed ultrasonically for 10 minutes. Then one or two drops of each of these suspensions were placed on a Carbon Type B, Au grid (300 mesh). Samples were ready for the test after evaporation of methanol. In this study, a JEOL 2010 transmission electron microscope (TEM) was used for imaging and SAED analysis.

2.3.4. Scanning Electron Microscopy (SEM)

For investigating the morphology and surface image of the sample particles SEM test was performed. The SEM images have the look of a traditional optical microscopic image but with much higher magnification.

In SEM, a source of electron which is focused in a probe scans the surface of the specimen and penetrates through the surface. In the meanwhile of penetration, the electrons are emitted from the surface of the specimen and are collected by detectors. The spatial resolution of this type of image will rarely be better than 0.5 μm.[26]

In this study a Zeiss EVO MA 15 SEM with LaB6 crystal source was used for SEM analysis. Samples were ready for test after grinding to a fine powder and being placed on a standard SEM stub.

2.3.5. Electron Dispersive X-ray Spectroscopy (EDX / EDS)

The EDX test is based on the X-ray production as a result of the ionization of an atom where the electron in the inner shell is removed. Afterward, an electron from a higher energy outer shell replaces the vacancy in the inner shell left from the ionization, and releases an amount of energy equal to the potential energy difference between the two shells. This excess energy, which is unique for every atomic transition, will be emitted by the atom either as an X-ray photon or will be self-absorbed and emitted as an Auger electron. Figure 2-3 illustrates the steps mentioned above:

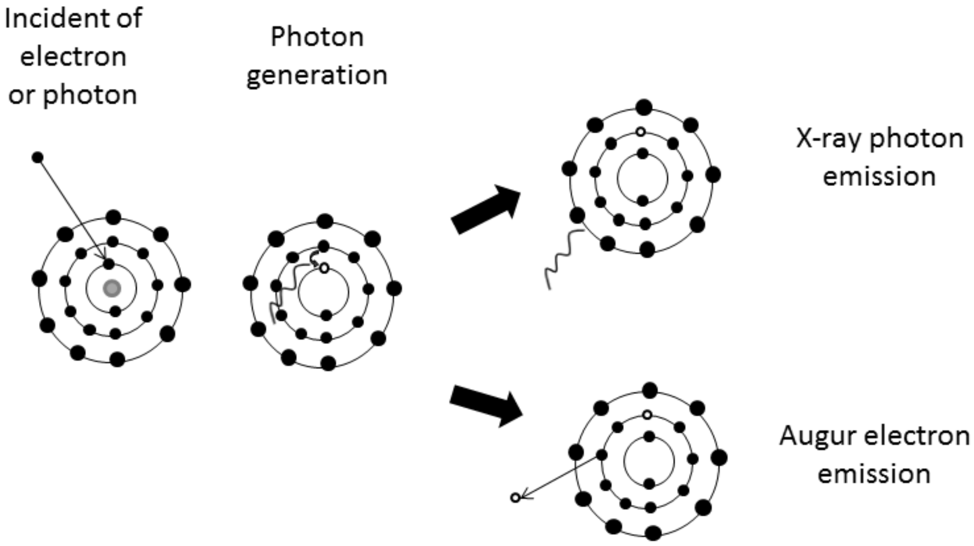

Figure 2-3 Emissions derived by atom ionization

For an atom with many shells, this emission occurs many times from a single ionization. The number and energy of the X-rays emitted from a specimen can be measured by an energy-dispersive spectrometer. Auger or photoelectrons can only escape from the uppermost atomic layers of the solid (depth of 10 nm or less), thus giving us information about the chemical elements in a materials' surfaces.[27]

The energy of the characteristic X-rays are equal to the energy differences between two electrons in different shells, which is well defined and in proportion with the atomic number of the atom. Thus all chemical elements can be identified with their characteristic X-rays, except the first three elements of the Periodic Table (H, He, and Li) which do not have enough electrons to produce characteristic X-rays.[26]

The energy-dispersive x-ray (EDX) detector is most commonly attached to SEM and TEM where the electron beams bombard the specimen and cause the characteristic X-ray emissions. The detector then converts X-ray energies into voltage signals; this information is sent to a pulse processor, which measures the signals and passes them onto an analyzer for data display and analysis.

In this study the elemental analysis of the samples was conducted simultaneously with the TEM test using the EDX spectrometers attached to the instrument.

2.3.6. X-Ray Photoelectron Spectroscopy (XPS)

XPS is applied to probe the elemental or chemical state in top 10 or so atomic layers within the surfaces (5-50 Å).[26] In XPS, soft x-rays with high energy (i.e. short wavelength) bombard the sample, causing electrons at different orbitals to be rejected. Einstein photoelectric law explains the mechanism:

$$KE = h\nu - BE \qquad \text{Equation 2.3}$$

where hν is the energy of the photon, BE is the binding energy of the particular electron and KE is the kinetic energy of the electron.

Electrons in orbitals with different energy levels produce different kinetic energies (KE), once exposed to photons with specified hν energy levels. While the intensity of this energy is measured (KE) it is converted to binding energies (BE) using the above equation.

The BE of an electron, as determined by the required energy for removing it from the atom, is equal to the energy level of each orbital which is specified for different orbitals in different atoms.

Core levels are energy levels assigned to electrons tightly bound to the nucleus and are specified for each atom in the periodic table. Thus, all the elements (except H and He) can be analyzed by comparing their core level BEs.

The chemical state of the atoms can be determined by XPS as well. Although the core level energy is constant for a single atom, it differs to some extent in different chemical states. Atoms of higher charges have higher valence charges (q), causing an increase in the potential (q/r; where r is the radius of the atom) felt by 1s orbitals. This results in higher BEs for the 1s energy level and determines the chemical state of the atom. The shift in the BEs of elements can be from 1 to several eVs, though it is very small in the case of copper and zinc. Table 2-1 lists the approximate BE shifts of various metals.[26]

Table 2-1 BE shifts in different chemical states of atoms

Element	Oxidation state	BE shift from zero-valent state
Ni	Ni^{2+}	~2.2 eV
Fe	Fe^{2+}	~3.0
	Fe^{3+}	~4.1
Ti	Ti^{4+}	~6.0
Si	Si^{4+}	~4.0
Al	Al^{3+}	~2.0
Cu	Cu^{+}	~0.0
	Cu^{2+}	~1.5
Zn	Zn^{2+}	~0.0
W	W^{4+}	~2.0
	W^{6+}	~4.0

While the core level electrons are ejected, there is a possibility of having an interaction with a valence electron (electrons of an atom that can participate in the formation of chemical bonds with other atoms). A photoelectron can excite a valence electron to an empty orbital of higher energy levels. This is known as shake-up process, where the photoelectron is ejected with less energy, thus the XPS peak moves to higher BEs (shake-up satellites).

For certain metals with unpaired electrons in 3d and 4f shells, the shake-up satellites produce strong peaks. The following figure (Figure 2-4) illustrates the 2p shake-up process in Cu^{2+} which can be applied as a tool for distinguishing Cu^{2+} in CuO from Cu^{+} in Cu_2O. The shift in BE of Cu^{+} and Cu^{2+} can also be used for copper state identification, but needs accurate BE measurements.

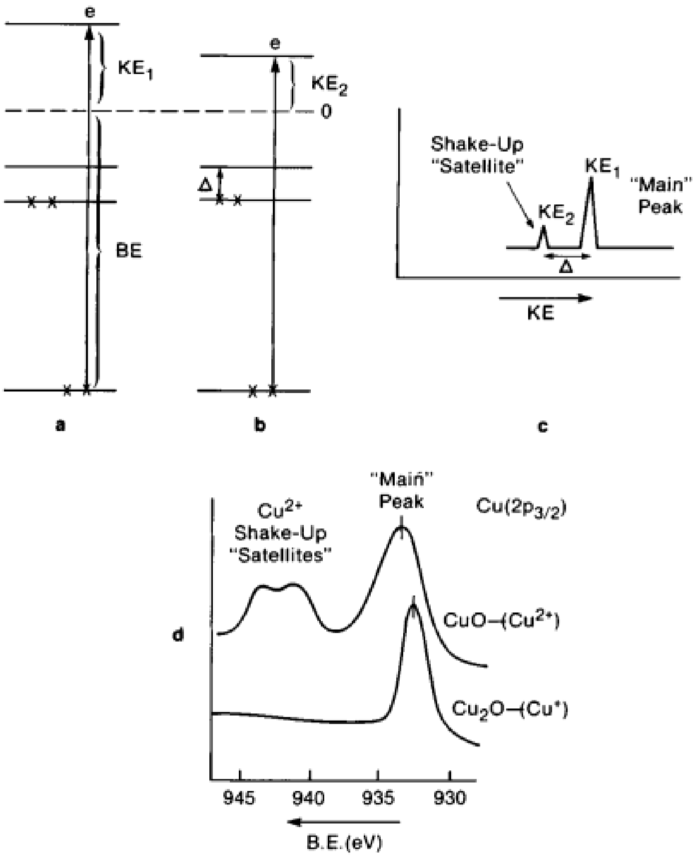

Figure 2-4 Shake-up peak appearance in Cu^{2+} XPS spectrum [26]

The XPS spectra show the photoelectron intensities versus binding energies, where the peaks come from photo-emission of either core level electrons or valence electrons and Auger emissions.

In this study, X-ray photoemission spectra were taken on an AXIS 165 spectrometer (Kratos Analytical). The base pressure in the analytical chamber was lower than 3×10^{-8} Pa. Monochromatic Al Kα source (hν = 1486.6 eV) was used at a power of 210 W. The analysis spot was 400 × 700 um. The resolution of the instrument was 0.55 eV for Ag 3d and 0.70 eV for Au 4f peaks. Vision-2 instrument software was applied to process the data. All spectra were calibrated for C1s binding energy position at 284.8 eV.

Since the peak positions in XPS spectra are sensitive to spectrometer conditions, there is a need for calibration before each test. The calibration was done with C 1s peak which can be found on the surfaces of all the samples exposed to air. The peak of core level binding energy of C1s is 284 and sufficiently unique to be used as a primary reference standard.

2.3.7. Thermal Analysis (TA)

In thermal analysis, changes in materials properties such as dimension, mass, phase and mechanical behavior are investigated as a function of temperature. The thermal events that can occur during heating of a solid at different temperatures are as follows:

1. Solid phase transformation
2. Glass Transition
3. Melting
4. Sublimation
5. Thermal decomposition

Thermogravimetric analysis (TGA) and Differential scanning calorimetry (DSC) are the most common analytical techniques in thermal analysis. TGA monitors the mass changes while DSC monitors the phase changes of the material with temperature.

In DSC, the first three of the thermal events mentioned above can be analyzed. These events do not include mass exchange with the surroundings and the observed difference between the reference material and the sample material is only caused by solid-state phase transformations and melting. On the other hand, TGA is an analytical technique which measures the mass change of a sample with temperature, thus can analyze material decomposition and thermal stability in a temperature range.

In DSC, there are two separate chambers for keeping the sample and reference. The instrument supplies the power for keeping the two chamber's temperatures the same. Thus when an endothermic event occurs in the sample, an increase in the power supply is observed and vice versa. The amount of power change is proportional to the energy of heat flux to compensate for the heat release or gain by the sample. The DSC curves are recorded by heating or cooling the sample with a constant rate in a temperature range.

In TGA, the mass change of the sample is recorded as a function of temperature. TGA instruments are composed of a microbalance for keeping the sample and recording the mass change, a furnace, temperature programmer and computer and samples in powder or pellet forms. The atmosphere for TGA test can be either reactive or non-reactive. In this study a TGA test was conducted with airflow to simulate the muffle furnace conditions during activation.

2.3.8. Atomic Absorption Spectrophotometry (AAS)

Atomic Absorption Spectrophotometry (AAS) is used for determination of the presence and concentration of about 70 elements of the periodic table. In this study, AAS was used to investigate the copper content (wt.%) in Cu-ETS-2, Cu-ETS-4 and Cu-ETS-10.

Each atom has sets of electrons, which are located at different levels with well-defined energies. While electrons move between energy levels, they absorb or emit energy equal to the energy difference between the levels (ΔE). The frequency of the light emitted is related to ΔE by the Einstein relation:

$$\Delta E = h \upsilon \qquad \text{Equation 2.4}$$

where h is the Planck's constant and υ is the frequency of the radiation, inversely proportional to wavelength. Each atom has a characteristic set of energy levels, thus has a particular set of frequencies in its atomic spectrum.

In AAS the sample solution is heated and decomposed to produce an atom cloud, known as atomization. In this study an Air-Acetylene flame was applied for atomization purposes. With proper flame conditions, most of the atoms in the atom cloud will remain in the ground state, thus can absorb light from a source lamp at the analytical wavelength (atomic absorption) and enter an excited state in the process. By measuring the amount of light absorbed, a quantitative determination of the amount of the element present can be made. In this study, the quantity of the sample was weighed using a balance with 0.1 mg resolution. Nitric acid was then added to the sample to extract the copper species and build-up 10 millilitres of solution. Then, the copper concentration in the solution was measured with VARIAN 220FS Atomic Absorption Spectrophotometer.

Chapter 3. Characterization of as-prepared Adsorbents before H_2S Exposure

3.1. Characterization of as-prepared ETS-2, ETS-4 and ETS-10

3.1.1. SEM Imaging

In order to investigate and compare the morphology and surface images of ETS-2, ETS-4 and ETS-10 particles, SEM test was performed and the images are shown in Figure 3-1, Figure 3-2 and Figure 3-3. The image magnification for ETS-2 is not within the same range as the image magnifications of ETS-4 and ETS-10. The particle size of ETS-2 sample is much smaller than particle size for ETS-4 and ETS-10, which necessitates a higher magnification for clearer image of the particles.

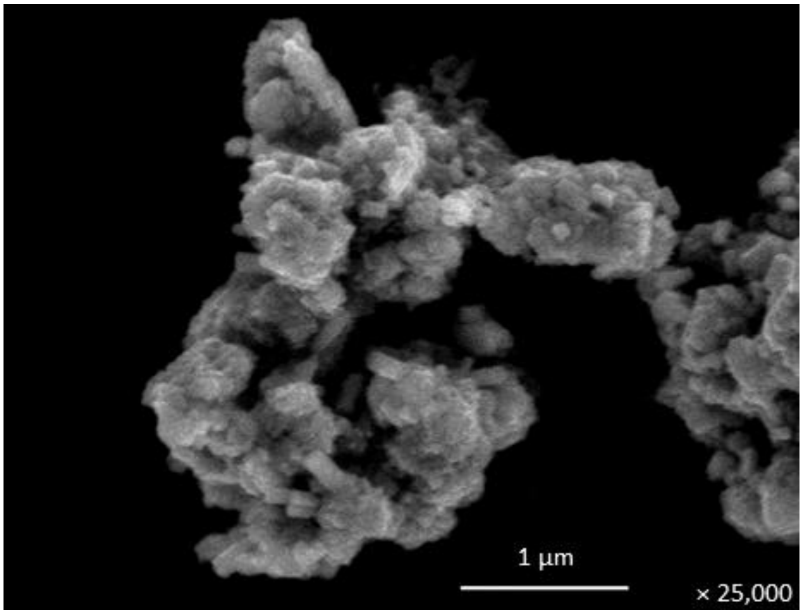

Figure 3-1 SEM image of ETS-2 particles

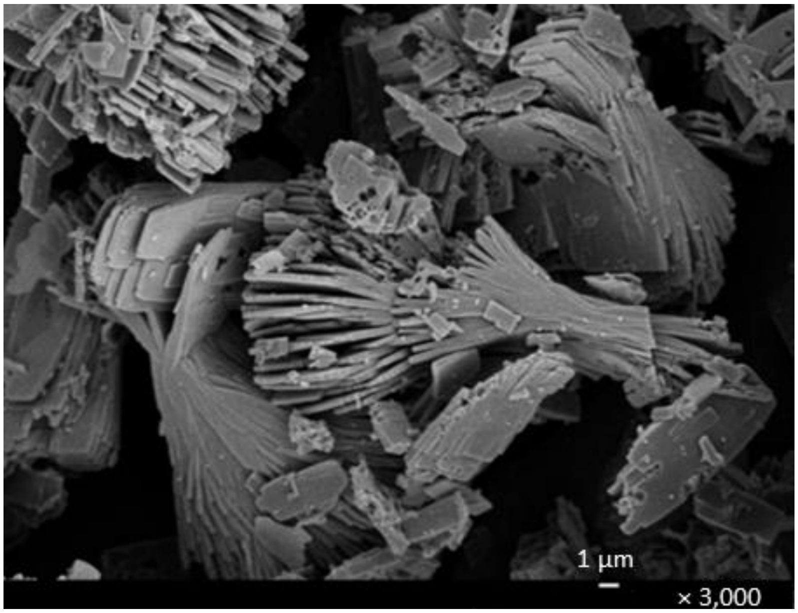

Figure 3-2 SEM image of ETS-4 particles

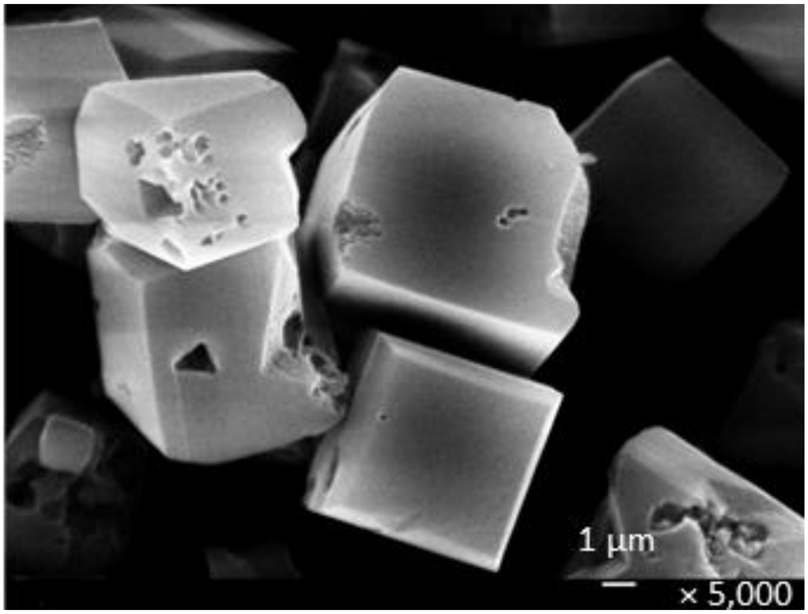

Figure 3-3 SEM image of ETS-10 particles

Taking into account the difference in magnification it can be seen that ETS-2 is composed of particles much smaller in size compared to ETS-4 and ETS-10. Based on Figure 3-1 ETS-2 appears to be constituted of two types of components, which agglomerate to form the clusters seen in the image.

3.1.2. TEM Imaging

In order to further investigate the components present in ETS-2, TEM images of the sample were also collected. For the test, the sample, in powder form, was suspended in methanol and then dispersed ultrasonically. This causes the separation to some extent of the agglomerated particles, and will help capturing the images of each component separately.

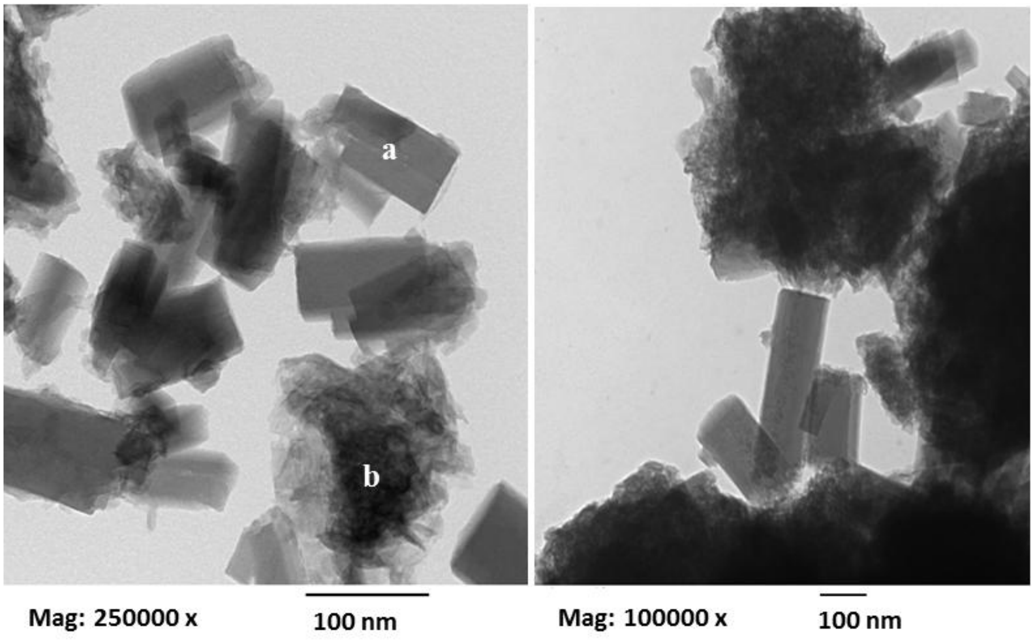

Figure 3-4 TEM images of as-prepared ETS-2

TEM images in Figure 3-4 confirm the existence of two types of components in ETS-2 (a and b).

3.1.3. EDX Analysis

To further analyze these components, elemental analysis was conducted using the Electron Dispersive X-ray Spectroscopy (EDX) instrument attached to TEM. Sodium to titanium and titanium to silicon ratios according to the elemental analysis for component "a" and 'b" were determined and are summarized in Table 3-1.

Table 3-1 Elemental ratios derived from EDX analysis results

	Component a	Component b
Na:Ti	0.04	0.49
Ti:Si	1.15	4.36

The results show that component ‘b’ has higher sodium to titanium ratio, and therefore will have a higher cation exchange capacity.

Thus, fine particles of ETS-2 are composed of two phases with different cation exchange capacities which are agglomerated together.

3.1.4. XRD Analysis

While SEM and TEM imaging techniques are useful for understanding the morphology and homogeneity of the sample, they give no direct information about the internal ordering of the crystallites.

To investigate the crystal structure and phase purity of the samples, powder x-ray diffraction test was performed. Figure 3-5 and Figure 3-6 depict the experimental (a) and simulated [28,29] (b) XRD patterns of ETS-4 and ETS-10 respectively. It can be seen that in both cases the material is highly crystalline and the reflections derived from XRD test (a) are an exact match of the simulated pattern (b).

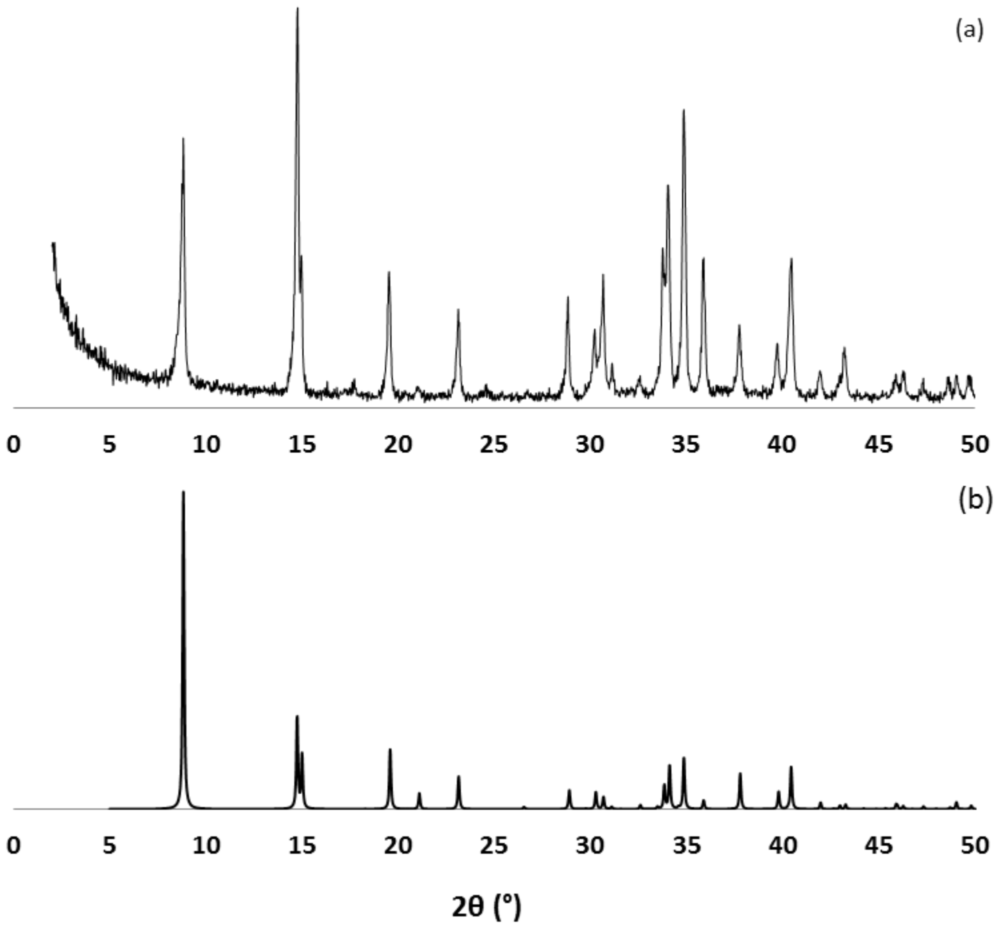

Figure 3-5 XRD pattern of ETS-4 (a) experimental, (b) simulated

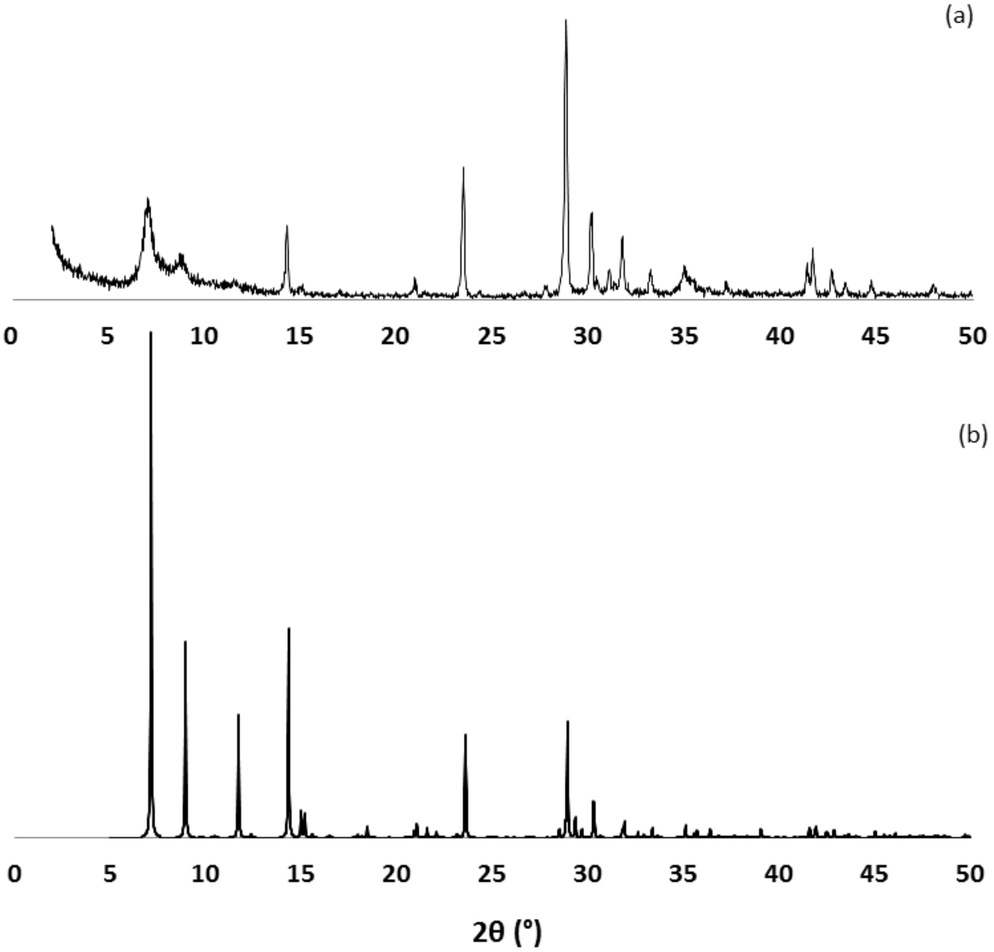

Figure 3-6 XRD pattern of ETS-10 (a) experimental, (b) simulated

In contrast, the XRD pattern of ETS-2 (Figure 3-7) shows few peaks with low intensities. The lack of a large hump between 20 and 40 degrees 2θ that is characteristic of amorphous materials, suggests that the sample is not entirely amorphous.

The broad peaks at 2θ of ~13, 32, 40 and 56 observed in XRD pattern of ETS-2 are a match for Titanium Hydrogen Oxide Silicate Hydrate ($H_4Ti_4O_4(SiO_4))_3.8H_2O$. However the most intense peak of the predicted composition at 2θ of 13.13 is significantly weakened in ETS-2. This may be due to the lack of homogeneity observed in ETS-2.

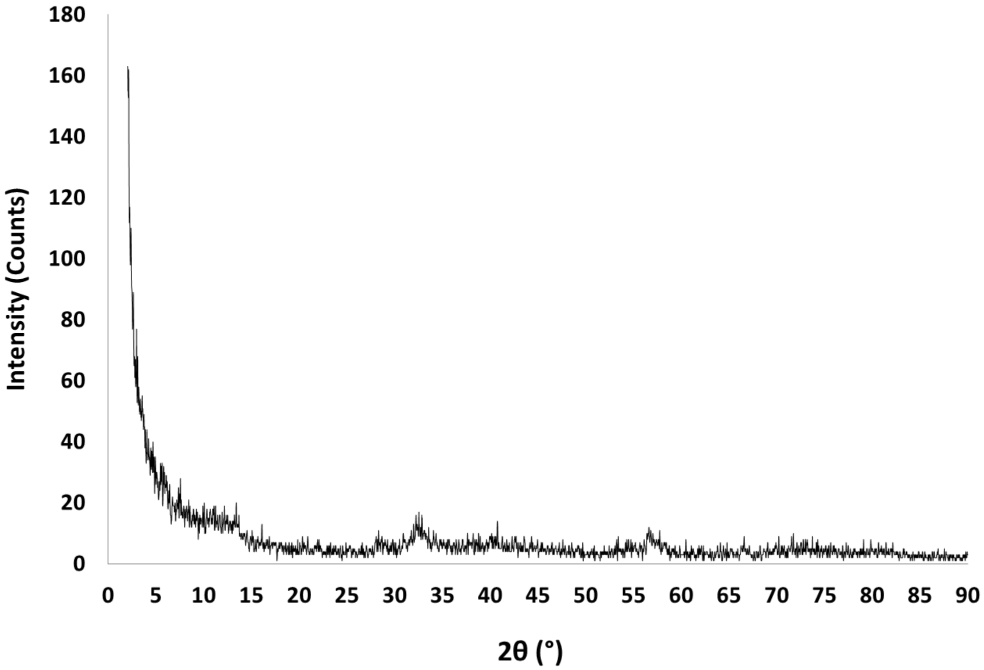

Figure 3-7 Experimental XRD pattern of ETS-2

3.1.5. SAED Analysis

In order to investigate the crystallinity of each component in ETS-2 selected area electron diffraction (SAED) of each component was collected with TEM. The results show that component ‘a’ is crystalline, while component ‘b’ is not. Thus, it can be concluded that in XRD pattern of ETS-2, the crystalline phase reflections were affected by the amorphous phase and therefore, the pattern lacks the well-defined, sharp peaks.

It can be concluded that ETS-2 is a semi-crystalline material (have both crystalline and amorphous components) with a higher Na/Ti ratio and cation exchange capacity in its amorphous phase.

3.1.6. Surface Area Measurements

The surface areas of the samples were measured by BET method using N_2 adsorption isotherms. Table 3-2 summarizes the surface area measurements of ETS-2 and ETS-10.

The surface area measurements cannot be performed for ETS-4, since the pores are too small to allow the N_2 molecules into the channels and collect the isotherm data.

Table 3-2 ETS-2 and ETS-10 surface area measurements

Sample	Surface area (m^2/g)	Internal surface (%)	External surface (%)
ETS-2	229	~0	~100
ETS-10	355	~90	~10

Although ETS-2 is not microporous, BET measurements indicate a relatively high surface area of 229 m^2/g. The high surface area in ETS-2 is the result of the external surface area of the very finely divided platelets. In contrast, the surface area for ETS-4 and ETS-10 is derived from their microporous structure and is almost entirely internal (~90 percent). The implication is that during ion exchange the exchanging cations would reside on the external surface area of ETS-2 and not within the pores and channels, as it is the case for ETS-4 and ETS-10.

3.2. Characterization of As-prepared Cu-ETS-2,Cu-ETS-4 and Cu-ETS-10

3.2.1. AAS Analysis

The copper cations were exchanged into ETS-2, ETS-4 and ETS-10 framework through the ion exchange procedure and pellets were prepared as mentioned earlier in Chapter 2. The copper content of the pellets of each sample was measured with atomic absorption spectrophotometry and the results are summarized in Table 3-3:

Table 3-3 Copper weight percent in adsorbents

Adsorbent	Copper (wt. %)
Cu-ETS-2	12.5
Cu-ETS-4	4.8
Cu-ETS-10	8.4

Although the same proportions of ETS-2/4/10 to copper nitrate salt were used during the ion exchange, different amounts of copper were loaded on each sample. Comparison of the copper loadings show that Cu-ETS-2 has the highest gravimetric copper loading and, assuming the same copper utilizations in all samples, will adsorb more H_2S.

3.2.2. TEM (Imaging and Diffraction) and EDX Analysis

Cu-ETS-2 was analyzed further in order to investigate morphology, crystal structure and the extent of exchange in its different components. Point specific analysis was conducted using EDX and TEM. The TEM images and SAED patterns of Cu-ETS-2 are shown in Figure 3-8:

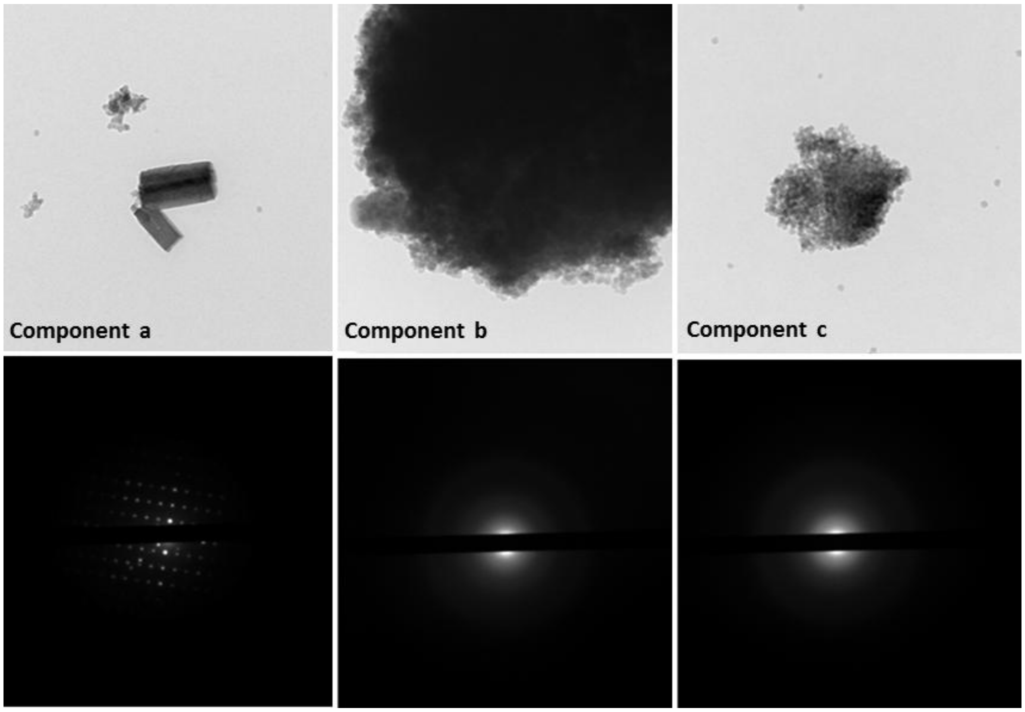

Figure 3-8 TEM images and SAED patterns of as-prepared Cu-ETS-2

Images show that components ‘a’ and ‘b’, observed in ETS-2, remain in the copper exchanged pellets. An additional amorphous component (c), which was not seen in the sample of as-synthesized ETS-2, is likely due to the addition of Ludox, a colloidal silica suspension, used in making the pellets.

Table 3-4 shows the point specific elemental analysis data of Cu-ETS-2 pellets collected by EDX attached to TEM. The atomic ratios of sodium to titanium, copper to titanium and titanium to silicon of each component are summarized in Table 3-5:

Table 3-4 Point specific elemental analysis of Cu-ETS-2

	Component a	Component b	Component c
Element	wt. %	wt. %	wt. %
Na	0.09	0.02	0.00
Si	0.32	0.52	1.00
Ti	0.58	0.39	0.00
Cu	0.01	0.08	0.00

Table 3-5 Elemental ratios derived from EDX analysis results

	Component a	Component b
Cu : Ti	0.01	0.15
Na : Ti	0.32	0.09
Ti : Si	1.06	0.44

EDX results (Table 3-4) show that Component ‘a’ has some un-exchanged sodium ions. Due to the low copper content, this component is not likely to be the active phase for H_2S adsorption.

The results also show that the third non-crystalline component, which was added during pelletizing, has no measureable copper content and therefore no H_2S adsorption potential.

As expected, most of the copper cations are deposited on the surface of component ‘b’. Table 3-5 shows that copper to titanium ratio in component ‘b’ is almost 10 times higher than for the component ‘a’ making this component the phase principally responsible for H_2S adsorption.

In conclusion, almost all the copper cations in ETS-2 are deposited in the component ‘b’, which lacks the pores and channels and whose surface area is all external. This means that the active copper phase in Cu-ETS-2 is more accessible for H_2S adsorption, in contrast to Cu-ETS-4 and Cu-ETS-10 where almost all the copper cations are deposited within the pores and channels.

3.2.3. XRD Analysis

XRD analysis was also conducted for Cu-ETS-2, Cu-ETS-4 and Cu-ETS-10 to investigate the crystal structure and phase purity of the samples (Figure 3-9, Figure 3-10 and Figure 3-11).

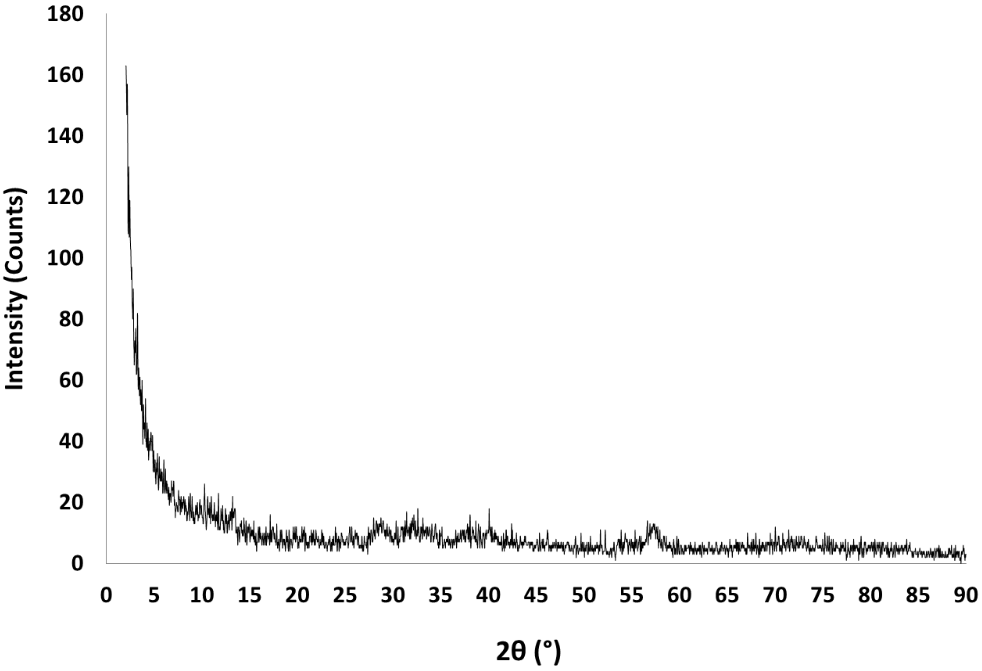

Figure 3-9 XRD pattern of Cu-ETS-2

Comparing the XRD pattern of Cu-ETS-2 (Figure 3-9) with XRD pattern of ETS-2 (Figure 3-7), it is clear that the copper exchange process does not introduce any significant changes in the ETS-2 structure. And since no diffraction peaks for copper compounds are detected in the XRD pattern of Cu-ETS-2 it also confirms the atomic-dispersion of copper ions in ETS-2 structure.

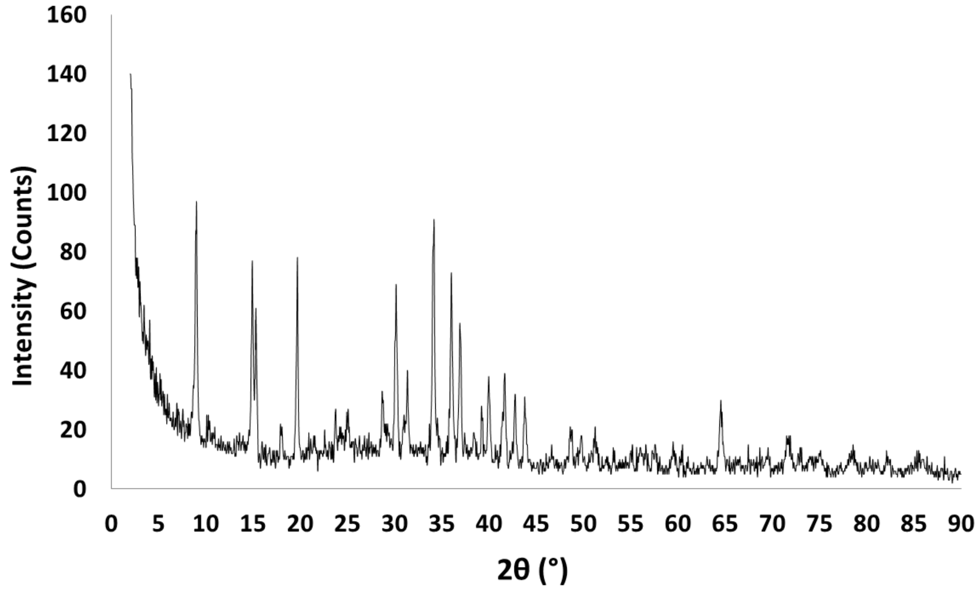

Figure 3-10 XRD pattern of Cu-ETS-4

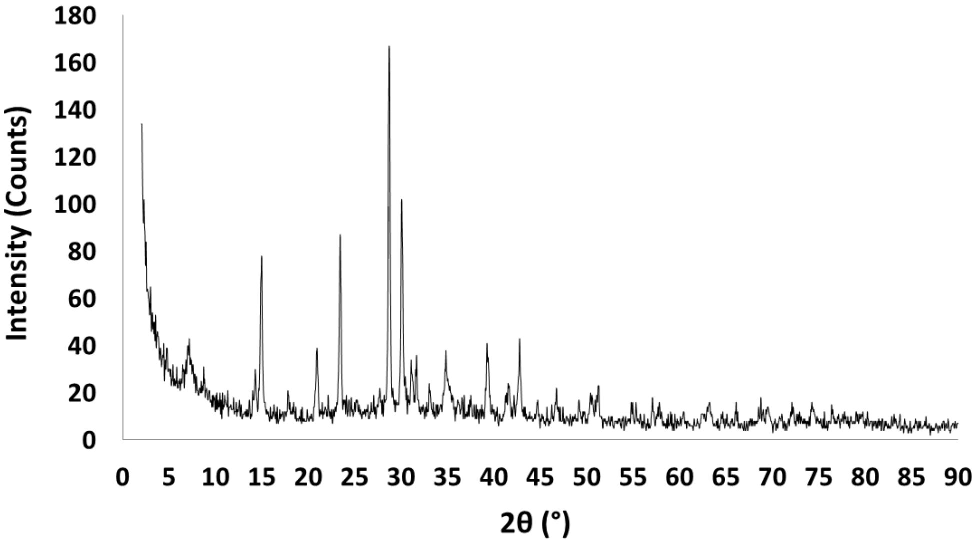

Figure 3-11 XRD pattern of Cu-ETS-10

XRD patterns of Cu-ETS-4 and Cu-ETS-10 (Figure 3-10 and Figure 3-11) show that the characteristic diffraction peaks of ETS-4 and ETS-10 are still detected. This means that the ion exchange has not affected the crystal structure of these materials.

In the case of Cu-ETS-4 and Cu-ETS-10, the reflections for copper compounds are visible. However, they mostly overlap with ETS-4 and ETS-10 reflections, and the atomic dispersion of copper species is anticipated in these frameworks as well.

3.2.4. XPS Analysis

To determine and compare the chemical state of copper species in Cu-ETS-2, Cu-ETS-4 and Cu-ETS-10, XPS test was conducted. Figure 3-12 shows the XPS spectra of Cu 2p region for the Cu-ETS-2 sample.

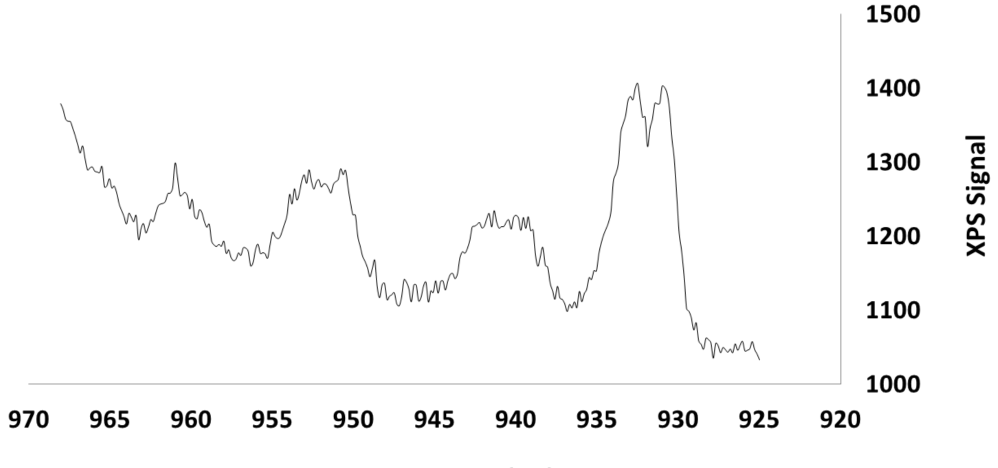

Figure 3-12 Cu-ETS-2 XPS Spectra, Cu 2p Region

The shake-up peak, characteristic of the divalent copper is visible in this spectrum. The shake-up peak at BE~ 941 eV and the peak at BE= 932.11 eV correspond to the divalent copper, whereas the peak at BE=930.06 corresponds to the monovalent copper. The latter was surprising since the samples were exchanged only with divalent copper. However the peak at BE of 930.06 eV could be explained by an artificial XPS-induced reduction of Cu^{2+} to Cu^{+} by X-rays, heat and secondary electrons as reported elsewhere.[30]

Since the binding energies of different copper compounds such as $Cu(OH)_2$, CuO, Cu_2O, Cu (metallic) are very close and cannot be distinguished, the only conclusion at this step is the existence of divalent copper, which is indicated by the shake-up peak. Auger Electron Spectroscopy was also used to investigate the copper's chemical state. However, the Auger lines of our samples were too small to be interpreted reliably.

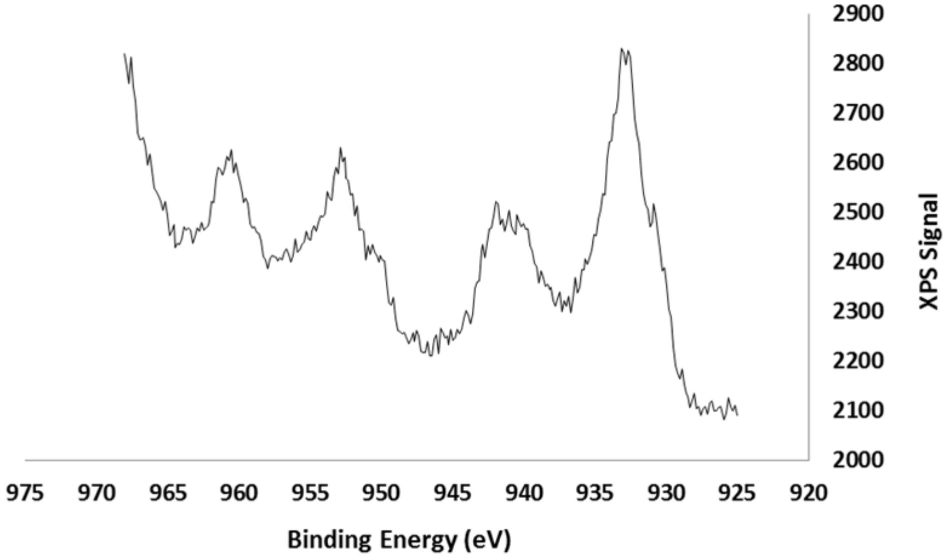

Figure 3-13 Cu-ETS-4 XPS Spectra, Cu 2p Region

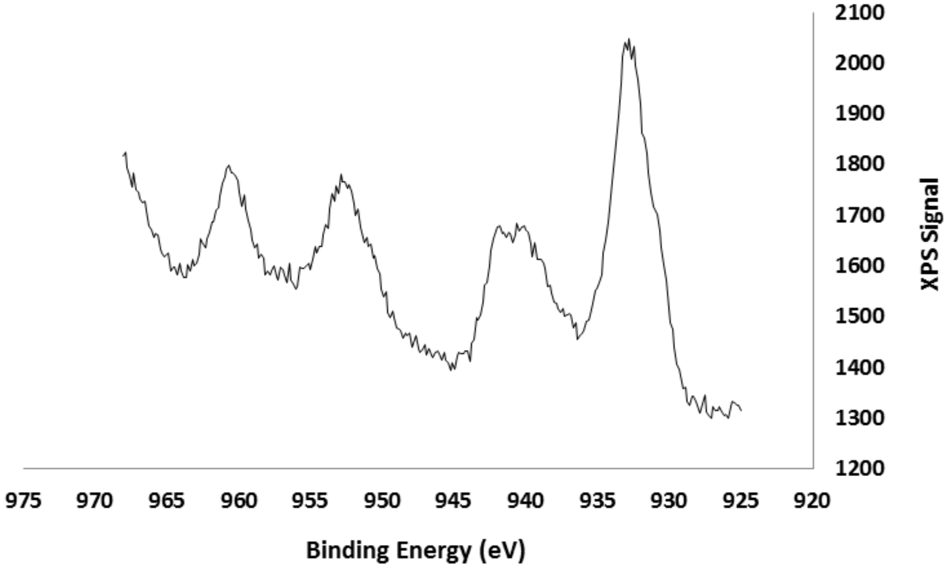

Figure 3-14 Cu-ETS-10 XPS Spectra, Cu 2p Region

The copper species in ETS-2 are in divalent chemical state and are similar to the ones in Cu-ETS-4 and Cu-ETS-10 (Figure 3-13 and Figure 3-14).

Thus, the same states of copper species were exchanged to ETS-2, ETS-4 and ETS-10 structures without affecting the original crystal structure of the material.

3.3. The Effect of Activation Temperature on Cu-ETS-2

3.3.1. XRD Analysis

In order to investigate the thermal stability of Cu-ETS-2, the XRD patterns of samples activated at different temperatures, were collected (Figure 3-15).

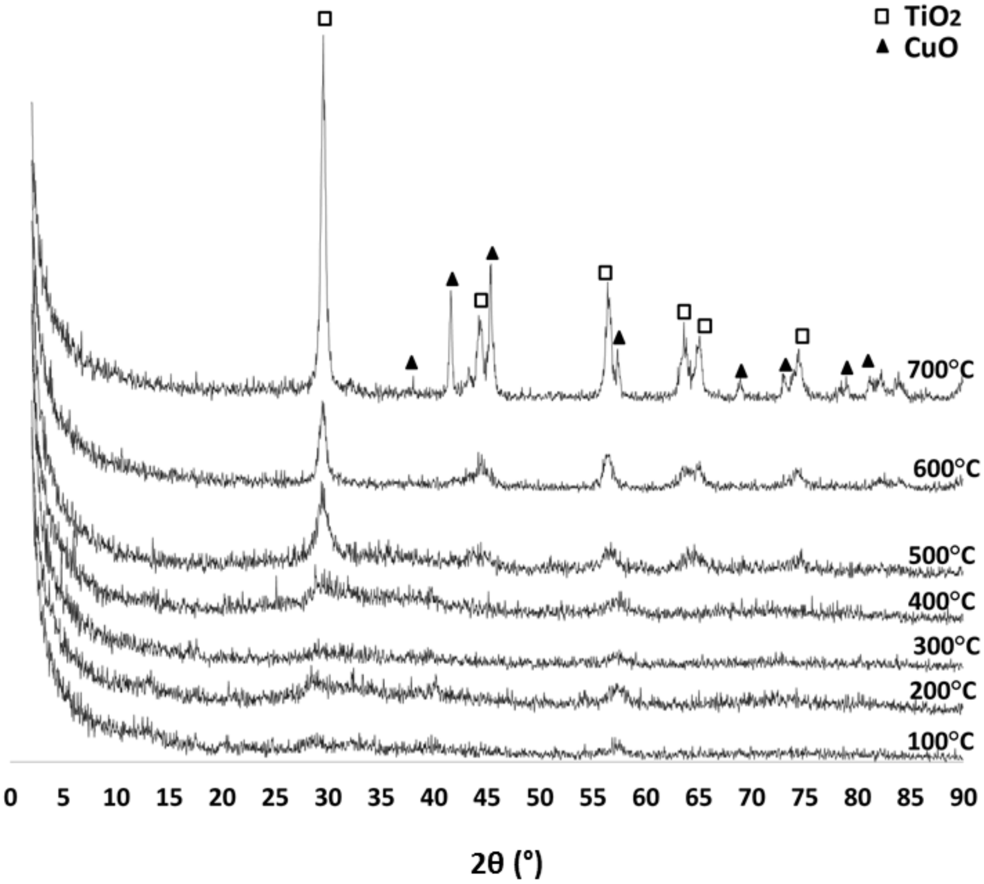

Figure 3-15 XRD pattern of Cu-ETS-2 activated at (100°C - 700°C)

The patterns in Figure 3-15 show that the semi crystalline framework of Cu-ETS-2 is stable up to 400°C. At temperatures above 400°C the characteristic reflections for Anatase (TiO_2) start to appear. At 700°C the characteristic reflections for CuO are seen, which suggests that highly dispersed copper ions have oxidized and sintered into agglomerates of copper oxide.

Thermal stability measurements for ETS-4 and ETS-10 have been reported in literature before. Naderi et al. investigated the thermal stability of ETS-4 by studying the XRD patterns of the sample activated at different temperature in air.[31] Naderi et al. showed that partial loss of crystallinity is observed at temperatures ≥ 200°C. The complete collapse of the crystalline structure was observed at 500°C. Thus copper exchanged ETS-4 cannot be stable at temperatures higher than 200°C. However, ETS-10 is stable at a wider temperature range, up to 550°C.[32] Another study also showed that copper exchanged ETS-10 is stable up to 550°C.[33]

Thus, the crystalline structure of ETS-4 and ETS-10, which brings about the atomic dispersion of copper species, is stable up to 200°C and 550°C, respectively. While the semi-crystalline structure of Cu-ETS-2 completely collapses at 700°C.

3.3.2. Surface Area Measurements

To investigate Cu-ETS-2 behavior at different activation temperatures, surface area measurements were also conducted (Table 3-6).

Table 3-6 Surface area measurements for Cu-ETS-2 activated at different temperatures

Activation temperature of Cu-ETS-2 (°C)	Surface area (m^2/g)
100	133.3
200	250.8
300	214.4
400	184.4
500	137.1
600	128.5
700	50.8

It is shown that the surface areas are within the same range for 100°C $\leq T \leq$ 600°C. Although the Anatase phase was observed at 500°C and 600°C, the surface area did not decrease significantly. An abrupt decrease in the surface area of the sample occurs at 700°C which coincides with the completion of crystallization and the appearance of copper oxide in the XRD patterns.

According to the surface area measurements at different activation temperatures and the abrupt decrease at 700°C, it can be inferred that the high surface area divided platelets are no longer present at this temperature.

3.3.3. TGA/DSC Analysis

The TGA/DSC test was also conducted for Cu-ETS-2 samples to track the crystallization events at different temperatures (Figure 3-16).

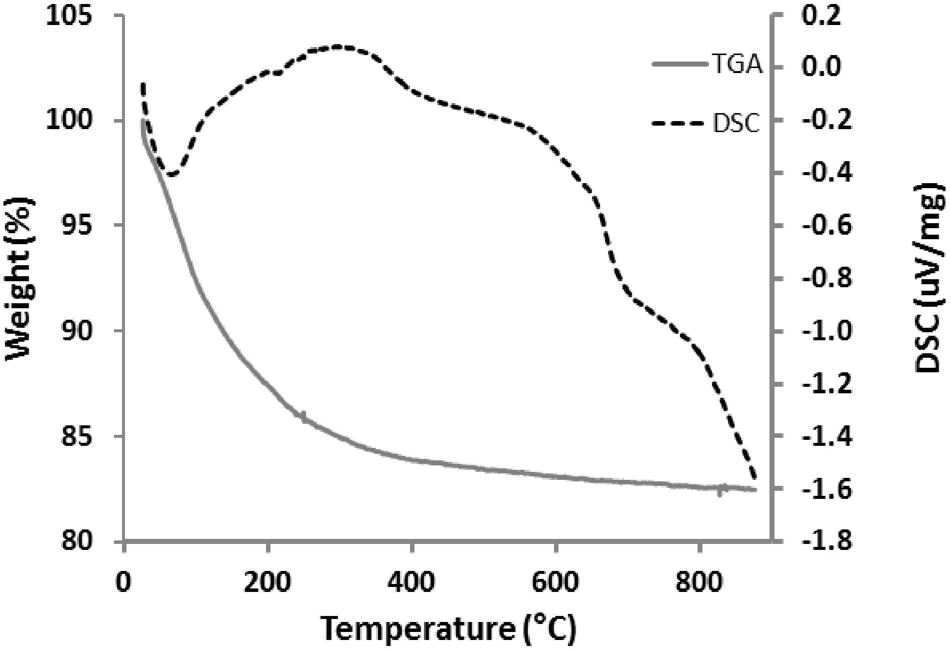

Figure 3-16 TGA/DSC curve of Cu-ETS-2 (ramp: 10°/min with air)

The TGA curve (solid line) shows one step mass loss of about 17 wt.% ,once the heating of the sample started. This is likely due to the loss in water content of the sample or any contamination adsorbed from the air (such as CO_2).

A well resolved endothermic peak at ~100° C in the DSC curve corresponds to dehydration, where the water content undergoes a phase change to vapor phase. There are also three broad exothermic peaks, which might correspond to crystallization or other possible phase changes in the sample. Since no crystallization was observed in the XRD of the sample activated at 200°C, the peak with the onset temperature of ~200°C in DSC is caused by a phase transformation event which has no crystallization. However the next two events with onset temperatures of T_c ~ 400° C and ~700° C correlate with the XRD patterns observed for Cu-ETS-2 activated at these temperatures. The lower temperature event is likely linked to the appearance of Anatase, while the event around 700 °C is probably due to CuO formation. Thus, the TGA/DSC curves support the previous observations for Cu-ETS-2 behavior at different activation temperatures.

In summary, ETS-2, ETS-4 and ETS-10 are high surface area ion exchangers that provide the atomic dispersion of copper cations in their framework and can be used for H_2S adsorption purposes. Cu-ETS-2 framework is different from that of Cu-ETS-4 and Cu-ETS-10. It lacks the pores and channels, and is entirely composed of an external surface area of fine platelets. In addition, Cu-ETS-2 can support more copper cations compared to Cu-ETS-4 and Cu-ETS-10. The unique morphology and structure of Cu-ETS-2 and dispersion of copper species remain relatively unchanged up to temperatures as high as 600°C. The next chapter would focus on the H_2S adsorptive properties of the materials discussed so far.

Chapter 4. H_2S Adsorption Experiments

H_2S removal capabilities of Cu-ETS-2, Cu-ETS-4 and Cu-ETS-10 are evaluated and compared against state of the art commercial H_2S adsorbent/polishers.

4.1. H_2S Adsorption on Cu-ETS-2,Cu-ETS-4 and Cu-ETS-10

H_2S adsorption tests were conducted for Cu-ETS-2, Cu-ETS-4 and Cu-ETS-10 in order to compare their H_2S breakthrough capacities (mg H_2S/g of adsorbent) and copper utilization (%). The breakthrough experiments were carried out using equivalent weights of adsorbent under the same test conditions as described in Chapter 2. The breakthrough time was defined as the time it took to register an outlet concentration of 0.5 ppm H_2S. The copper utilization was calculated by converting the breakthrough capacity to moles of H_2S, and then dividing that value by the moles of copper on the adsorbent sample, as measured by the AAS test. Table 4-1 summarizes the results for breakthrough capacities as well as copper utilizations.

Table 4-1 Cu-ETS-2, Cu-ETS-4 and Cu-ETS-10 comparison

Adsorbent[a]	H_2S breakthrough capacity (mg H_2S/g of adsorbent)	Copper loading wt.%	Copper utilization %
Cu-ETS-2	47	12.5	71
Cu-ETS-4	11	4.8	44
Cu-ETS-10	45	8.4	98

[a] All adsorbents were activated at 100°C

Results show that Cu-ETS-4 has the lowest copper utilization. This can be explained by a pore blockage effect. In crystalline materials with very small pores and channels, such as ETS-4, the copper sites nearest the external surface of the crystals are the first to react with H_2S to form copper sulfide. As a result the occluded sulfur partially blocks the pore openings, impeding the gas access to the rest of the crystal.[14]

The copper utilization data further supports this explanation. Cu-ETS-10 which has larger pore openings than Cu-ETS-4 has a higher copper utilization. The larger pore diameter in ETS-10 allows for the gas passage even if the channel is partially occluded. The almost complete utilization of copper species in Cu-ETS-10 is caused by the atomic dispersion of copper species in its microporous framework.

The data also shows a substantial (71%), but incomplete, copper utilization for Cu-ETS-2. This could be due to the heterogeneity in the sample structure that may not allow some of the exchanged copper ions to react with H_2S, or may be the result of active copper sites being blinded due to copper sulfide formation on the surface of the particles.

4.2. Cu-ETS-2 versus Cu-ETS-10

Although Cu-ETS-10 displayed the highest copper utilization, Cu-ETS-2 is preferred for H_2S adsorption for a couple of reasons.

First, the existence of pores and channels in microporous materials, such as Cu-ETS-10, can be problematic in humid gas streams, as the pore system will fill up with liquid water due to capillary condensation and the adsorbent will be unable to react with H_2S directly from the gas stream. This capillary condensation is not predicted however for Cu-ETS-2 since it lacks the microsporous structure and is composed entirely of the external surface area.

Second, the exchange capacity of ETS-2 is higher than that of ETS-10. (Copper loading of 12.5 wt.% versus 8.4 wt.%). This means that by improving ETS-2 structure to gain higher utilization, higher capacity is also expected for Cu-ETS-2.

For these reasons Cu-ETS-2 has the potential to be an effective H_2S adsorbent and be applicable even under industrial conditions of humid gas streams.

4.3. Cu-ETS-2 versus Commercial Samples

After its identification as a possible candidate for polishing gas streams out of H_2S in industrial applications, Cu-ETS-2 was compared to commercial H_2S scrubber/polisher (BASF Company). List of the commercial samples from BASF and their compositions are summarized in Table 4-2.

Table 4-2 Commercial samples (BASF Company)

Commercial sample	Composition
R3-12	40 wt. % CuO + 40 wt. % ZnO
R3-11G	36 wt.% CuO
ZnO	Pure ZnO

Zinc oxide and copper oxide both have spontaneous reactions with H_2S at room temperature, as depicted in the reactions below and can be applied for scavenging H_2S out of gas streams at room temperature. [2]

$$CuO(s) + H_2S\ (g) \rightarrow CuS\ (s) + H_2O\ (l) \qquad \Delta G\ (298\ K) = -126\ kJ/mol$$

$$ZnO(s) + H_2S\ (g) \rightarrow ZnS\ (s) + H_2O\ (l) \qquad \Delta G\ (298\ K) = -76\ kJ/mol$$

However, thermodynamic is just a tool for predicting the reactions. Other parameters can affect the adsorbent capacity and utilization of the samples.

The H_2S adsorption test was conducted under the same conditions using the same amount (50mg) for all three commercial adsorbents and Cu-ETS-2 (Figure 4-1).

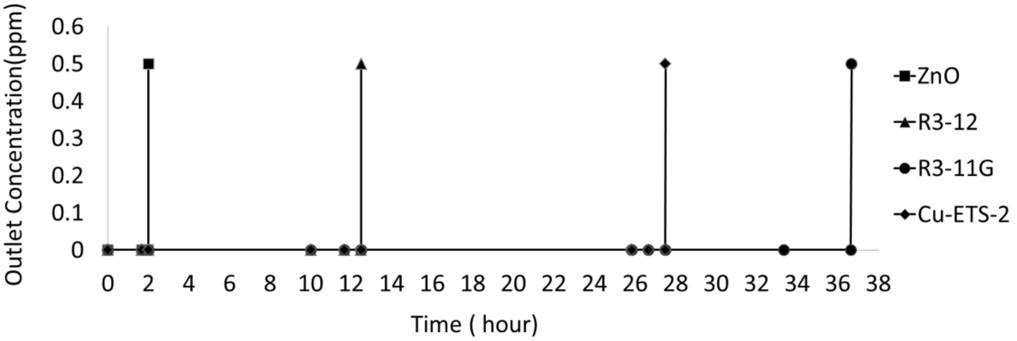

Figure 4-1 Comparison of the breakthrough times for 50 mg of Cu-ETS-2 and commercial H_2S adsorbents

The results show that under the specified test conditions, Cu-ETS-2 (activated at 100°C), has superior H_2S breakthrough capacity compared to the ZnO and R3-12 commercial adsorbents. It is also capable of maintaining a column outlet concentration of H_2S of less than 0.5 ppm for ~27 hours. The only commercial sample with longer breakthrough time is R3-11G with 36 wt.% copper oxide.

Surface area measurements were conducted for these samples and the results are summarized in Table 4-3.

Table 4-3 Specific surface area of commercial samples versus Cu-ETS-2

Sample	Specific surface area (m^2/g)
Cu-ETS-2	133.3
R3-11G	151.2
R3-12	117.8
ZnO	27.9

From the combined data it is clear that the breakthrough times and H_2S breakthrough capacities are proportional to the specific surface area of the samples. ZnO has the lowest surface area and the lowest H_2S capacity, while R3-11G has the highest surface area and the highest H_2S capacity.

Table 4-4 summarizes the utilization of active species (copper/zinc) for all the samples tested.

Table 4-4 Copper/zinc utilization

Adsorbent	Loading wt.%		% Utilization
	Copper	Zinc	
Cu-ETS-2	12.5	-	71
R3-11G	28	-	43
R3-12	32	32	6.5
ZnO	-	80	0.8

The data shows that, despite having the highest surface area and capacity, R3-11G suffers from low utilization of copper species (43%). It also shows that Cu-ETS-2 has the highest utilization amongst all the samples. The significant improvement in Cu utilization in Cu-ETS-2 compared to the rest of the samples is caused by an increase in the degree of dispersion of active species on the ETS-2 support via ion-exchange.

Once the copper species on the external surface of CuO particles in R3-11G sample are exposed to H_2S gas molecules, the sulfur layer is formed and blocks the rest of the centered CuO active species. Figure 4-2 shows that a significant amount of CuO species in R3-11G remains unreacted after H_2S exposure. In Cu-ETS-2 on the other hand, all the active species are deposited on the external surface of the inert support (ETS-2) and are consumed due to the H_2S exposure.

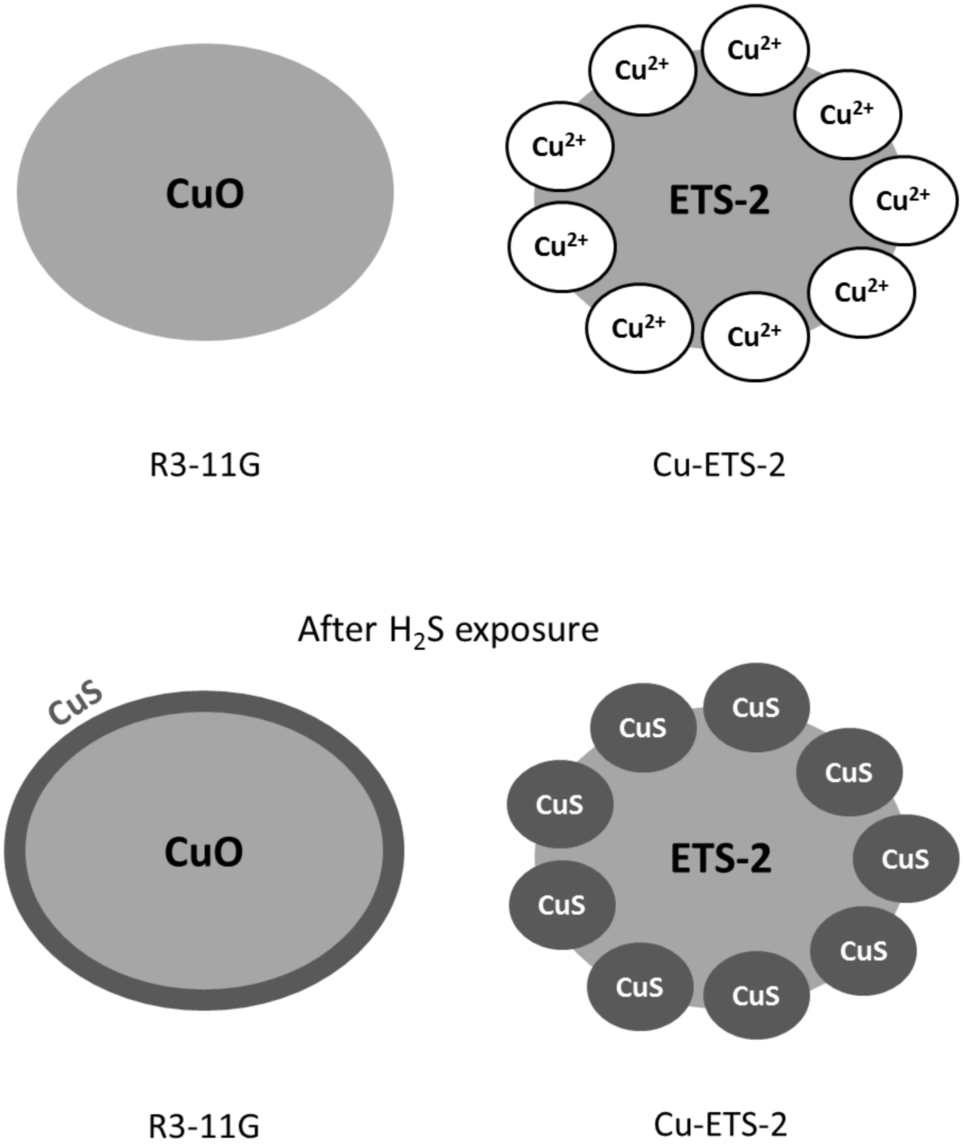

Figure 4-2 Schematic of Cu-ETS-2 and R3-11G particles before and after H_2S exposure

In conclusion, high surface area is essential for high capacity, but it does not guarantee a high utilization. A high dispersion of active species is the essential requirement for high utilization. R3-11G for example, which has a higher surface area and capacity than Cu-ETS-2 has only 43 percent utilization (Table 4-4) since it lacks the high dispersion parameter.

ETS-2 with its high surface area and ion exchange capacity allows the high dispersion of copper species on the external surface of its finely divided platelets, and thus is an appropriate substrate for a copper-based H_2S adsorbent.

4.4. The Effect of Activation Temperature on H_2S Capacity of Cu-ETS-2

In order to investigate the effect of activation temperature on H_2S breakthrough capacity of Cu-ETS-2, H_2S adsorption tests were conducted for samples activated at different temperatures. Figure 4-3 summarizes the breakthrough capacities of samples under the same test conditions, at room temperature.

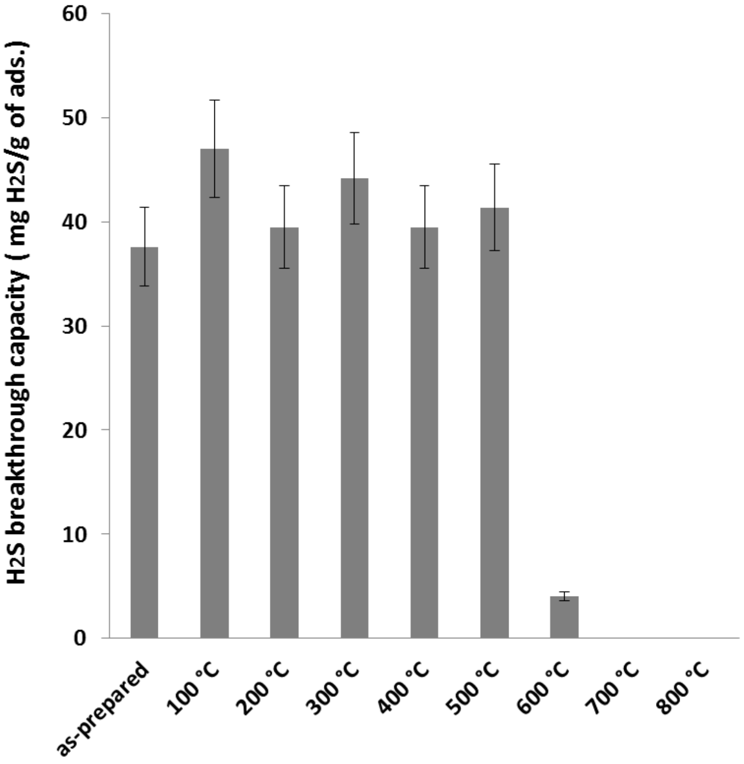

Figure 4-3 Breakthrough capacity of Cu-ETS-2 activated at different temperatures

Figure 4-3 shows that the high H_2S capacity of Cu-ETS-2 remains relatively unchanged up to an activation temperature of 500°C. Beyond this temperature there is a sharp decrease in capacity at 600°C, and no adsorption capacity at higher temperatures (over 700°C). The decrease in capacity beyond 500 °C seems to be associated with an increase in the amount of anatase phase (as seen in the XRD patterns) and could be assigned to a re-crystallization event which appears to render the adsorbent inactive toward H_2S (Figure 3-15, Chapter 3).

The complete loss in H_2S capacity of Cu-ETS-2 at 700°C is due to a complete loss in the atomic dispersion of copper species at this temperature. According to XRD results (Figure 3-15, Chapter 3) at 700°C the framework components are crystallized and the copper ions are oxidized (CuO) and sintered.

Although the copper oxide (CuO) particles are reactive toward H_2S in R3-11G sample, they do not adsorb measurable amounts of H_2S in the case of Cu-ETS-2 activated at 700°C. There are several possible explanations for this loss in capacity:

- The surface area of Cu-ETS-2 activated at 700°C is much lower than that of R3-11G (50.8 m^2/g versus 151.2 m^2/g). In addition, not all the measured surface area for heterogeneous Cu-ETS-2 sample is derived from copper oxide species. Thus the actual surface areas of CuO particles in Cu-ETS-2 are even lower than 50.8 m^2/g.
- The copper oxide particles could have been blinded by other non–reactive components of heterogeneous Cu-ETS-2 during recrystallization events. This makes the active CuO particles in Cu-ETS-2 inaccessible to H_2S gas molecules and renders the adsorbent inactive.

In summary, Cu-ETS-2 has a high H_2S capacity derived from its semi-crystalline structure, up to temperatures as high as 500°C. This wide temperature range of thermal stability, defines the applicable range for Cu-ETS-2 sulfidation and regeneration. Regeneration of the adsorbent was beyond the scope of this study and was not attempted.

4.5. The Effect of Copper Exchange Ratios on H_2S Capacity of Cu-ETS-2

To investigate the optimum ratio for copper exchange onto ETS-2, an ion exchange procedure was conducted with different ratios of ETS-2 to copper nitrate salt and the H_2S capacities for each ratio were measured (Table 4-5).

Table 4-5 H_2S capacity of Cu-ETS-2 for different exchange ratios of copper

ETS-2 : $Cu(NO_3)_2$ ratio (wt/wt)	H_2S breakthrough capacity (mg H_2S/g of ads.)	% Decrease in capacity
1 : 2	47	Reference
1 : 1	45	4%
1: 0.35	29	38%

The data suggests that the amount of copper salt can be reduced to half the commonly used amount, without a change in the H_2S breakthrough capacity. However, further decrease of copper salt cause 38% loss in H_2S capacity. Thus the optimum ratio for copper exchange onto ETS-2 appears to be one to one ratio.

4.6. The Effect of Gas Mixture on Cu-ETS-2 Adsorptive Performance

In addition to PEM fuel cell applications, which require a polishing bed for purifying their feed gas, Cu-ETS-2 can be applied for H_2S removal in different industries. CO_2 capturing, which is one of the research topics pursued by the Helmholtz-Alberta Initiative projects [34], focuses mainly on reducing the CO_2 emissions produced in processing of the bitumen. However, scavengers, such as Cu-ETS-2, are required to remove contaminants from gas streams to separate pure CO_2 suitable for compression and storage. Pure CO_2 reduces eventual compression costs and eliminates other liquification and storage issues.

In order to evaluate Cu-ETS-2 capabilities for removing H_2S out of CO_2, adsorption test were conducted with H_2S diluted in CO_2 instead of N_2.

The GC/FPD instrument used for H_2S concentration measurements used in this study could not separate H_2S from CO_2. A simple gas monitor which could detect 1 ppm H_2S with the lowest limit of 3 ppm was used instead. In order to validate this method a comparison was made by repeating the experiment with the gas monitor for H_2S in N_2 as well (Figure 4-4).

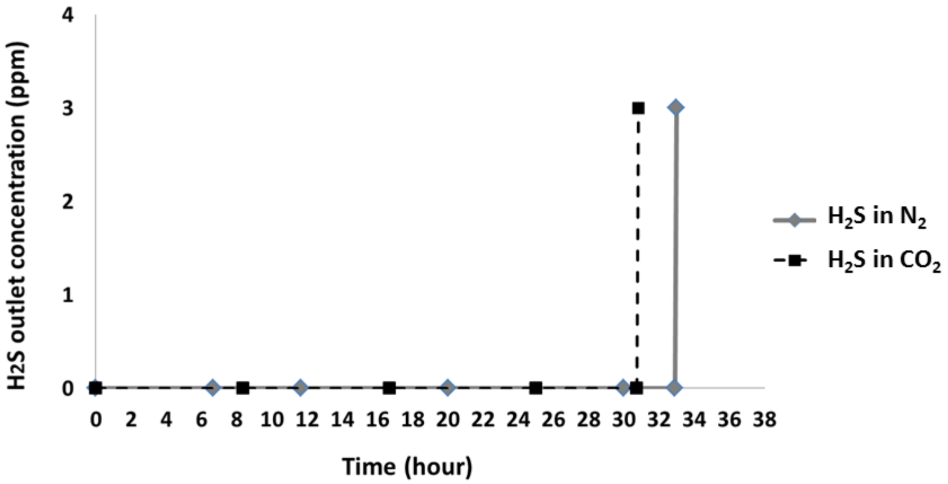

Figure 4-4 H_2S breakthrough point (3 ppm) for N_2 and CO_2 gas streams

The results show approximately the same breakthrough times for both gas mixtures. Within the experimental errors associated with testing, these results show that CO_2 has no interference with H_2S adsorption on Cu-ETS-2.

Thus Cu-ETS-2, stable at temperatures as high as 500°C, is a promising adsorbent for removing H_2S out of gas streams. In addition the H_2S capacity and copper utilization of Cu-ETS-2 are superior compared to the commercial samples tested in this study.

Chapter 5. Conclusion and Recommendations

H_2S is a major contaminant in different gas streams with negative consequences such as pipeline corrosion and catalyst poisoning, even at very low levels. Conventional techniques for H_2S removal are: absorption in liquids (alkaloamines, ammonia solutions, and alkaline salt solutions), the Claus Process, and reaction on activated carbons or metal oxides. Among the above mentioned techniques, reactive removal of H_2S with metal oxides is the most promising for polishing gas streams down to sub-ppm levels of H_2S. While much is known for metal oxides with desulfurization potentials at high temperatures (>350°C), metal oxides' desulfurization capabilities at lower temperatures (room temperature) are not well investigated. H_2S removal at room temperature is essential for technologies such as on-board fuel processing of PEM fuel cells, since their anode Pt catalysts is susceptible to H_2S at levels as low as 0.1-1 ppm.

Cu-based compounds have been shown to have superior H_2S adsorption performance at room temperature. Therefore copper was chosen as the active species for H_2S adsorption and was loaded on different supports in order to improve capacity and utilization.

ETS-2, ETS-4 and ETS-10 are high surface area ion exchangers and were evaluated as supports for copper species. Atomic dispersion of the same copper species was observed in all the samples without detectable changes in the crystal structure of the supports. However, in some aspects Cu-ETS-2 was different than

Cu-ETS-4 and Cu-ETS-10. The difference is attributed to the special crystal structure and morphology of ETS-2 particles. The high surface area of ETS-2 comes from the external surface area of the semi-crystalline finely divided platelets. Thus all the copper species are deposited on the external surface of the particles and are exposed to H_2S gas molecules.

The high surface area of ETS-4 and ETS-10 mostly comes from the surface area within the pores and channels, hence is mostly internal. The internal deposition of copper species was determined to be problematic for H_2S removal in the case of Cu-ETS-4, since the pore blockage limited the copper utilization significantly. However, Cu-ETS-10 had almost complete utilization of copper species, which correlates with its bigger pore size.

Cu-ETS-2 was found to be superior over Cu-ETS-10 for H_2S removal purposes. Lack of pores and channels in Cu-ETS-2 structure eliminates the capillary condensation issues in humid gas streams. In addition, it has higher copper loading compared to Cu-ETS-10, which means a higher H_2S capacity when complete utilization of copper species occurs.

H_2S removal capacity of Cu-ETS-2 was also higher when tested against commercial H_2S scrubbers (ZnO and R3-12) at room temperature. The only commercial sample that had slightly higher H_2S breakthrough capacity was R3-11G (36 wt.% CuO) that had lower copper utilization. This implies that the high dispersion of copper species on the ETS-2 fine particles significantly improves the utilization of copper species.

Cu-ETS-2 also showed a wide range of thermal stability up to 500°C. At higher temperatures a crystallization event happens and renders the adsorbent totally inactive toward H_2S at 700°C. In addition, the presence of CO_2 in the gas streams does not affect the H_2S adsorptive performance of Cu-ETS-2. In summary this study shows that Cu-ETS-2 is a promising adsorbent for polishing H_2S streams at room temperature.

The work presented in this thesis can be further expanded into ways to increase copper loading on ETS-2, such as increasing the ETS-2 phase purity. Another area with future potential is exchanging other metals onto ETS-2 and investigate other temperature ranges for H_2S adsorption.

References

(1) Stirling, D. Sulfur Problem - Cleaning up Industrial Feedstocks, **2000**.

(2) Baird, T.; Denny, P. J.; Hoyle, R.; McMonagle, F.; Stirling, D.; Tweedy, J. Modified Zinc-Oxide Absorbents for Low-Temperature Gas Desulfurization. *Journal of the Chemical Society-Faraday Transactions* **1992**, *88*, 3375-3382.

(3) Gangwal, S. K. In Desulfurization for Fuel Cells; Fuel Cells: Technologies for Fuel Processing; Elsevier: Amsterdam, **2011**; pp 317-360.

(4) Health and Safety Fact Sheet, Hydrogen Sulfide. http://cupe.ca/health-and-safety/Hydrogen_Sulfide (Accessed November 1, 2011).

(5) Huang, C.; Chen, C.; Chu, S. Effect of moisture on H_2S adsorption by copper impregnated activated carbon. *J. Hazard. Mater.* **2006**, *136*, 866-873.

(6) Westmoreland, P. R.; Harrison, D. P. Evaluation of candidate solids for high-temperature desulfurization of low-Btu gases. *Environ. Sci. Technol.* **1976**, *10*, 659.

(7) Elseviers, W. F.; Verelst, H. Transition metal oxides for hot gas desulphurisation. *Fuel* **1999**, *78*, 601-612.

(8) Yang, H. Y.; Tatarchuk, B. Novel-Doped Zinc Oxide Sorbents for Low Temperature Regenerable Desulfurization Applications. *AICHE J.* **2010**, *56*, 2898-2904.

(9) Ayala, R. E.; Marsh, D. W. Characterization and Long-Range Reactivity of Zinc Ferrite in High-Temperature Desulfurization Processes. *Ind Eng Chem Res* **1991**, *30*, 55-60.

(10) Abbasian, J.; Hill, A. H.; Wangerow, J. R.; Flytzani-Stephanopoulos, M.; Bo, L.; Patel, C.; Chang, D. Development of novel copper-based sorbents for hot-gas cleanup. Final technical report, September 1, 1991--August 31, 1992.

(11) Lew, S.; Sarofim, A. F.; Flytzani-Stephanopoulos, M. Sulfidation of zinc titanate and zinc oxide solids. *Ind Eng Chem Res* **1992**, *31*, 1890-1899.

(12) Ko, T.; Chu, H.; Chaung, L. The sorption of hydrogen sulfide from hot syngas by metal oxides over supports. *Chemosphere* **2005**, *58*, 467-474.

(13) Gasper-Galvin, L.; Atimtay, A. T.; Gupta, R. P. Zeolite-supported metal oxide sorbents for hot-gas desulfurization. *Ind Eng Chem Res* **1998**, *37*, 4157-4166.

(14) Kyotani, T.; Kawashima, H.; Tomita, A.; Palmer, A.; Furimsky, E. Removal of H_2S from Hot Gas in the Presence of Cu-Containing Sorbents. *Fuel* **1989**, *68*, 74-80.

(15) Krumpelt, M.; Krause, T. R.; Carter, J. D.; Kopasz, J. P.; Ahmed, S. Fuel processing for fuel cell systems in transportation and portable power applications. *Catalysis Today* **2002**, *77*, 3-16.

(16) Chunshan, S. Fuel processing for low-temperature and high-temperature fuel cells: Challenges, and opportunities for sustainable development in the 21st century. *Catalysis Today* **2002**, *77*, 17-49.

(17) Xue, M.; Chitrakar, R.; Sakane, K.; Ooi, K. Screening of adsorbents for removal of H_2S at room temperature. *Green Chem.* **2003**, *5*, 529-534.

(18) Kuznicki, S. M. CHE 584 Class Notes, Molecular Sieve Technology, University of Alberta, Winter 2010.

(19) Cronstedt, A. Akad. Handl. **1756**, 18, 120.

(20) Baerlocher, C.; McCusker, L. B.; Olson, D. H. In Atlas of Zeolite Framework Types; Elsevier: Amsterdam, **2007**.

(21) Mer'kov, A.N.; Bussen, I.V.; Goiko, E.A.; Kul'chitskaya, E.A.; Men'shikov, Yu.P.; Nedorezova, A.P. Raite and zorite-new minerals from the Lovozero Tundra. *Zapiski Vsesoyuznogo Mineralogicheskogo Obshchestva*, **1973**, 102, 54-62 (in Russian).

(22) Kuznicki, S. M. U.S. Patent No. 4,853,202 ,1989.

(23) Lopes, C. B.; Coimbra, J.; Otero, M.; Pereira, E.; Duarte, A. C.; Lin, Z.; Rocha, J. Uptake of Hg^{2+} from aqueous solutions by microporous titano- and zircono-silicates. *Química Nova* **2008**, *31*, 321-325.

(24) Fagerlund, G. Determination of specific surface by the BET method. *Mater. Struct.* **1973**, *6*, 239.

(25) Brunauer, S.; Emmett P. H.; and Teller, E. Adsorption of Gases in Multimolecular Layers. J. Am. Chem. Soc., **1938**, 60, 309-319.

(26) Brundle, C. R.; Evans, C. A. J.; Wilson, S. Encyclopedia of Materials Characterization - Surfaces, Interfaces, Thin Films. **1992**.

(27) Leng, Y. In *Materials characterization : introduction to microscopic and spectroscopic methods;* J. Wiley: Singapore; Hoboken, NJ, **2008**.

(28) Nair, S.; Jeong, H.; Chandrasekaran, A.; Braunbarth, C. M.; Tsapatsis, M.; Kuznicki, S. M. Synthesis and Structure Determination of ETS-4 Single Crystals. Chem. Mater. **2001**, 13, 4247-4254.

(29) Anderson, M. W.; Terasaki, O.; Ohsuna, T.; Philippou, A.; MacKay, S. P.; Ferreira, A.; Rocha, J.; Lidin, S. Structure of the microporous titanosilicate ETS-10. Nature **1994**, 367, 347-351.

(30) Schlesinger, R.; Klewe-Nebenius, H.; Bruns, M. Characterization of artificially produced copper and bronze patina by XPS. *Surf. Interface Anal.* **2000**, *30*, 135-139.

(31) Naderi, M.; Anderson, M. W. Phase transformation of microporous titanosilicate ETS-4 into narsarsukite. *Zeolites* **1996**, *17*, 437-443.

(32) Anderson, M. W.; Terasaki, O.; Ohsuna, T.; Malley, P. J. O.; Philippou, A.; Mackay, S. P.; Ferreira, A.; Rocha, J.; Lidin, S. Microporous titanosilicate ETS-10: A structural survey. *Philosophical Magazine Part B* **1995**, *71*, 813-841.

(33) Gervasini, A.; Picciau, C.; Auroux, A. Characterization of copper-exchanged ZSM-5 and ETS-10 catalysts with low and high degrees of exchange. *Microporous and Mesoporous Materials* **2000**, *35-36*, 457-469.

(34) The Helmholtz-Alberta Initiative. http://www.helmholtzalberta.ca/ (Accessed November 1, 2011)